



University of
Massachusetts
Amherst

Point of Care Diagnostics and Health Monitoring Devices

Item Type	Dissertation (Open Access)
Authors	Shanmugam, Akshaya
DOI	10.7275/7899360.0
Download date	2026-03-07 08:59:02
Link to Item	https://hdl.handle.net/20.500.14394/19829

POINT OF CARE DIAGNOSTICS AND HEALTH MONITORING DEVICES

A Dissertation Presented

by

AKSHAYA SHANMUGAM

Submitted to the Graduate School of the
University of Massachusetts Amherst in partial fulfillment
of the requirements for the degree of

DOCTOR OF PHILOSOPHY

February 2016

Electrical and Computer Engineering

© Copyright by Akshaya Shanmugam 2016

All Rights Reserved

POINT OF CARE DIAGNOSTICS AND HEALTH MONITORING DEVICES

A Dissertation Presented

by

AKSHAYA SHANMUGAM

Approved as to style and content by:

Christopher D. Salthouse, Chair

Paul Siqueira, Member

Wayne P. Burleson, Member

Sam R. Nugen, Member

Christopher V. Hollot, Department Head
Electrical and Computer Engineering

To
Amma, Appa, Deeps, Lokesh, and Bambi
For everything.

ACKNOWLEDGEMENTS

I give me great pleasure to thank those who have made this thesis possible. I owe my deepest gratitude to Professor Christopher Salthouse, who made available his support in every possible way. Time and again Prof. Salthouse has gone that extra mile to make sure that I get the best out of the program and my time at UMass. He has had a strong influence on my professional life by being a dedicated guide, motivating teacher, and an inspiring mentor. I extend my gratitude to the committee members, Professor Paul Siqueira, Professor Wayne P. Burleson, and Professor Sam Nugen for their valuable time, suggestions, and encouragement. It has been a pleasure discussing research with such an accomplished panel.

I thank the Nugen research group, Rotello lab, and Professor Donna M Zucker for their significant additions to this work. I would like to thank my lab mates Shuo Li, Hongtao Wang, Addison Mayberry, and Yamin Thuzar Tun for their contribution toward this thesis. Working alongside colleagues who were always happy to help and share their knowledge in their field of expertise has aided in advancing this thesis in many ways. I would also like to thank Prasana Ravindran, Arun Saranathan, Moumita Ray, Varun Srinivasan, and Baird Soules for taking time to offer their thoughts and suggestions. I am indebted to all my friends for their emotional support through thick and thin.

I am sincerely grateful to the Hluchyjs, the Isenberg family, and the UMass innovation challenge for facilitating my research work. These awards have led to exciting collaborations and allowed me to explore new dimensions of my research. I would also like to thank the department and the UMass community for making my time at UMass a great experience.

Lastly, and more importantly I would like to thank my family for all that they have done and continue to do. I wish to thank my sister for showing me how to face the unpredictability of life with strength, elegance, and compassion. I am eternally grateful to my parents Geetha Shanmugam and Shanmugam Duraisamy for all that they sacrificed to offer us nothing but the best. Their trust, confidence, and unconditional love has been a huge source of motivation. I thank Lokesh Subramany for his patience, kindness, and for offering nothing but love and support toward my personal and professional endeavors. I am fortunate to have them in my life; to them I dedicate this thesis.

ABSTRACT

POINT OF CARE DIAGNOSTICS AND HEALTH MONITORING DEVICES

FEBRUARY 2016

AKSHAYA SHANMUGAM, B.E., ANNA UNIVERSITY

M.S., UNIVERSITY OF MASSACHUSETTS, AMHERST

Ph.D., UNIVERSITY OF MASSACHUSETTS, AMHERST

Directed by: Professor Christopher D. Salthouse

Existing disease screening methods mostly rely on symptom based diagnosis. This is mainly because of lack of accessibility and cost associated with the tests. Testing for the presence of the disease after the onset of symptoms has a negative impact on chances of survival and treatment costs.

Miniaturized low cost diagnostic devices that can be used outside the hospital setting can provide continuous health monitoring and aid in early diagnosis. This thesis presents techniques to develop such disease screening and health monitoring devices. The techniques presented here focus on medical devices that can benefit from microfluidic devices, fluorescence imaging, and antibody testing.

TABLE OF CONTENTS

	Page
ACKNOWLEDGEMENTS.....	v
ABSTRACT.....	vii
LIST OF TABLES.....	x
LIST OF FIGURES.....	xi
 CHAPTER	
1. INTRODUCTION.....	1
2. HEAT SENSITIVE ADHESIVE TAPE MICROFLUIDIC DEVICE ON CMOS.....	4
2.1 Problem statement.....	4
2.2 Literature review.....	5
2.3 Project outline.....	7
2.4 Methods.....	7
2.4.1 Fabrication of HSA microfluidic device on a glass substrate	7
2.4.2 Fabrication of HSA microfluidic device on CMOS sensor	9
2.4.3 Fabrication of PSA and PDMS microfluidic devices	10
2.5 Results.....	12
2.5.1 Pressure test	12
2.5.2 Surface roughness.....	15
2.5.3 Edge uniformity	16
2.6 Conclusions	20
3. ON-SENSOR FLUORESCENCE IMAGING DEVICE FOR SCREENING BLOOD	21
3.1 Problem statement	22
3.2 Literature review.....	23
3.3 Project outline.....	25
3.4 Methods.....	25
3.4.1 Device calibration	26
3.4.2 Lensless fluorescence imaging.....	26
3.5 Results.....	29
3.5.1 Results with flow applications	30
3.6 Conclusions	30
4. SINGLE USE LOW COST ASSAY FOR HEPATITIS C SCREENING.....	32
4.1 Problem statement	34
4.2 Literature review.....	34
4.3 Project outline.....	36
4.4 Methods.....	37
4.4.1. Human factor study	37
4.4.2. Electrode design	41
4.4.3. Functionalization protocol.....	42
4.4.4. PCB design.....	43
4.4.5. Microfluidic fabrication.....	45

4.4.6. Microcontroller and Matlab code.....	46
4.5 Results.....	49
4.5.1 Saline solution.....	49
4.5.2 Protein detection.....	51
4.5.3 Protein detection with commercial electrodes.....	54
4.6 Conclusions.....	55
5. CONCLUSION.....	57
REFERENCES.....	59

LIST OF TABLES

Table	Page
1. Speed, power, and run settings on the laser cutter used in patterning the tape for microfluidic fabrication.....	17

LIST OF FIGURES

Figure	Page
1. Anatomy of the heat seal adhesive tape [25].....	8
2. HSA microfluidic device fabricated on a glass substrate (A) HSA device (B) HSA+PDMS device.....	9
3. HSA microfluidic device fabricated on a bare CMOS sensor (A) HSA device (B) HSA+PDMS device.....	10
4. PSA and PDMS microfluidic devices (A) PSA device on a glass substrate (B) PDMS device on a glass substrate (C) PSA device on CMOS (D) PDMS device on CMOS	12
5. Pressure measurement set-up to quantify the amount of pressure a microfluidic device can withstand	13
6. Pressure test for HSA, PSA, PDMS, and HSA+PDMS devices on a glass slide. The columns represent the mean pressure and the error bars represent the standard deviation	14
7. Pressure test for HSA, PSA, PDMS, and HSA+PDMS devices on a CMOS sensor. The columns represent the mean pressure and the error bars represent the standard deviation	14
8. Surface height variation on HSA, PSA, and PDMS. The graph shows the mean and the standard deviation.....	15
9. Stages in the Matab code for quantifying edge variation. (A) Original image (B) Image after edge detection (C) Identifying boundaries (D) Boundary with best fit line	18
10. Edge variations in glass fabricated devices.....	19
11. Edge variations in CMOS fabricated devices.....	19
12. Illustration of lensless imaging [44]	24
13. Effect of sample sensor separation on lensless fluorescence imaging.....	25
14. Calibration graph that relates the signal strength and the height of the sample [45].....	26
15. PSA microfluidic device fabricated on a bare CMOS sensor for lensless imaging [46].....	27
16. Imaging set up to perform lensless imaging [46].....	28
17. Consecutive frames of sample flowing inside a PSA microfluidic device. (A-C) fluorescent beads (D-F) cells stained with fluorescent dyes [45].....	29
18. Sample tracking using lensless fluorescence imaging device	30
19. Data collected from the human factor study. Columns represent the mean and error bars represent standard deviation for each step in screening.....	39
20. Interdigitated electrodes (A) PCB design (B) Fabricated electrodes	41
21. Illustration of gold electrodes with self-assembled monolayer and green fluorescent protein	42
22. Printed circuit board to conduct electrochemical impedance spectroscopy.....	44

23. Topology used for measuring impedance change in electrodes	45
24. Microfluidic device on PCB for sample containment.....	46
25. Original data points and interpolated data points	47
26. Maxima and minima points on input and output signals	48
27. EIS results from NaCl with different concentrations (A) Amplitude spectrum (B) Phase spectrum (C) Nyquist plots.....	50
28. Plots comparing the values from an oscilloscope and the proposed device (A) Output voltage (B) Phase difference	51
29. Contact angle on gold surface (A) Bare gold electrodes (B) Gold electrodes after the formation of SAM	52
30. Protein detection using proposed device (A) Amplitude spectrum (B) Phase spectrum (C) Nyquist plot	53
31. Protein detection using proposed device and commercial electrodes	55

CHAPTER 1

INTRODUCTION

Diseases have existed longer than humans; disease diagnosis can be dated back to 400 BC, when the oldest known diagnostic test was performed. The test involved pouring urine on the ground and observing if it attracted insects. During the middle ages and the seventeenth century, studying body fluids, mainly urine was the predominant technique for diagnosis. In 1754, clinical diagnostics by measuring heart rate, blood pressure, and temperature was refined. By 1850, stethoscopes, ophthalmoscopes, and laryngoscopes were used in clinical examination. The next huge stride in diagnosis was the invention of microscopes, X-ray, chemical tests, and bacteriological tests. Diagnostic techniques picked up in the mid-1800s with the invention of new devices and establishment of hospital labs [1].

These days there are a plethora of clinically used diagnostic tools and tests. Diagnostic tests can be broadly classified as belonging to biochemistry, hematology, microbiology, radiology, and pathology. Specialized equipment and set-ups are currently used to perform these tests to diagnose an array of diseases. At hospitals, tests are usually ordered to determine the cause of illness after patients show symptoms. These tests range from minimally invasive tests such as blood tests and physical examination, to more invasive procedures such as angiography and biopsy [2] [3].

Proper diagnosis plays a defining role in medical costs associated with treatment and effectiveness of the treatment. Although existing screening methods have worked well, diagnosis is usually performed only after symptoms start to appear. Life threatening diseases such as

cancer, HIV, hepatitis C, heart diseases, and stroke show very few or no symptoms in the early stages. They are diagnosed by an observant eye during an annual general health checkup, or in most cases undiagnosed till the health of the individual has been adversely affected. This uncertainty has cost thousands of lives every year; heart diseases, cancer, and stroke are among the top five causes of death contributing to about 1,302,200 deaths each year in the US [4]. These diseases also pose a huge economic burden to the country; more than 75% of the health care expenditure in the US is on people with chronic conditions [5].

Mobile health monitoring and hand held devices can solve this problem by providing personalized care. The wide spread use of such technology has enabled the use of medical devices outside hospitals and clinics. Devices with a wide range of complexity such as temperature sensors, heart rate monitoring devices, calorie counters, sugar level monitor, blood pressure monitor, and activity monitoring devices are commercially available today. The use of mobile devices such as mobile phones, smart phones, and other mobile communication technologies in the recent past has garnered huge interest and has led to the emergence of the field known as mHealth [6] [7]. Some groups have also developed systems for monitoring various biological signals to provide more information on an individual's health [8]. The global market for medical devices in 2013 was 348 billion dollars and has an average growth of 3% each year [9].

This thesis presents 3 key techniques: microfluidic fabrication for miniaturized sensors, miniaturized fluorescence imaging system, and a point of care hepatitis C screening device. Microfluidic devices aid in sample delivery and housing the sample under study in most miniaturized devices. New microfluidic fabrication techniques are required for different applications. The second chapter discusses the fabrication techniques for developing microfluidic

devices directly on CMOS sensors. These devices can be used for optical examination of sample or integrated with existing chemical sensors for disease screening, bio sensing, cytological studies, and sample flow imaging to name a few.

The third chapter presents a lensless fluorescence imaging device capable of detecting and quantifying the fluorescence signal of sample. The specificity of fluorescence imaging is currently used in labs to diagnose many types of cancers, AIDS, and other blood related disorders. This device can be employed in clinical application that require qualitative and quantitative data from fluorescently stained sample.

The proof of concept for a novel hepatitis C screening device is presented in chapter four. This device will be capable of detecting the antibody in blood, detecting the virus, and classifying the virus subtype. The proposed device overcomes the drawbacks of conventional screening devices and techniques. The functionality of the presented screening technique can also be employed to screen other diseases and detect various biomolecules.

This thesis proposal presents a detailed literature review and results for each of these projects. The aim of this work is to develop alternate techniques and methods that aid in the advancement of health monitoring and disease screening. Applications for the techniques presented in this thesis are numerous. Low cost technologies that can provide continuous health monitoring, and portable screening devices will reform the healthcare industry in the US.

CHAPTER 2

HEAT SENSITIVE ADHESIVE TAPE MICROFLUIDIC DEVICE ON CMOS

Microfluidic devices have played a critical role in miniaturization of numerous devices by providing a means for sample delivery. Microfluidics perform complex tasks such as mixing, focusing, and growing live cells on miniaturized devices [10] [11] [12]. Some applications of microfluidics include gene chips, labs on a chip, chemical sensors, flow controllers, micronozzles, and microvalves. In the United States alone, the field of microfluidics has grown to be a \$4.45 billion market [13].

Most microfluidic devices consist of 3 layers: the base forms the foundation of the microfluidic device, a middle layer that channels the flow of the sample, and a top layer to seal the microfluidic chamber. In some devices, the function of the middle layer is performed by the top or the bottom layer. Conventionally, microfluidic devices are built on glass or plastic substrates and an external imaging device is employed for sample analysis. By building microfluidic devices on integrated circuits (IC), sample sensing can be performed on chip.

2.1 Problem statement

The fragility, small size, and uneven surface of CMOS makes fabrication of microfluidics on CMOS more difficult than glass. Interaction of subsystems, aqueous nature of biological samples, and device yield also pose constraints to the integration of the system. This chapter describes a low cost, high yield technique for the integration of microfluidics and CMOS. Techniques to improve performance parameters such as capability to sustain pressure and methods to produce uniform channel edges are also presented.

2.2 Literature review

Conventional microfluidic devices built on glass slides are usually fabricated using a technique known as soft lithography. In this technique a master mold is created and the microfluidic device is made out of a polymer known as Poly(dimethylsiloxane) (PDMS). The polymer has a refractive index of 1.41 and is optically transparent from 240 to 1100 nm; this makes optical imaging, fluorescence imaging, and coupling with light possible. PDMS is flexible, conforms to surfaces, and can be released from molds without being damaged. This property of PDMS greatly simplifies the fabrication process. The flexible nature of the polymer makes it capable of handling pressure and stress without cracking or breaking. PDMS can also be integrated with circuits as it is electrically insulating. The polymer is nontoxic, inert, permeable to gas, and has low permeability to liquid making it compatible with cells and proteins [14]. To fabricate the device, the polymer is poured over the master and cured to define the channels. The PDMS is then peeled and adhered to a glass slide.

These conventional fabrication techniques do not scale well for IC fabrication, hence other techniques such as removal of bulk material [15], surface micromachined channels [16], and SU-8 devices [17] were developed. In bulk removal technique, the silicon substrate is patterned using a series of photolithography and etching steps. A silicon dioxide layer is used as an etch mask and the pattern is defined using a photoresist. The oxide is removed to form the walls of the microfluidic chambers. Pyrex glass is then bonded to the silicon to seal the chambers. Surface micromachining can be used to develop channels in a variety of materials. With a polymer, a thin layer is deposited on the prefabricated IC. A photoresist layer defines the channel dimensions and another polymer layer is patterned to form the walls of the microfluidic chambers. The photoresist layer is then sacrificed. SU-8 is a photodefinable photoresist; to create microchannels,

a thin layer is coated on the surface and developed. This forms the walls of the channels and the top layer is formed by bonding. These devices are mechanically reliable, and have good chemical resistance. This technique also provides control over the height of the channel; the thickness of the SU-8 layer defines the channel height.

Once the microfluidic device is developed, it has to be bonded to a surface; in this case, complementary metal-oxide-semiconductor (CMOS). Existing bonding techniques can be classified as direct or indirect. Anodic bonding and fusion bonding are direct bonding techniques. Anodic bonding requires the surfaces to be cleaned extensively and employs high voltage and high temperature to form an irreversible bond. Fusion bonding works by application of extensive pressure after cleaning in vacuum. The substrate is then exposed to heat to form a stronger bond. Adhesive bonding, eutectic bonding, solder bonding, and thermocompression bonding are types of intermediate layer bonding. Epoxy, spin-on-glass, or UV curable glue is spin coated on the surface during adhesive bonding. In eutectic bonding, a thin gold layer is placed between the silicon layers and heated to gold-silicon eutectic point to form an irreversible bond. Thermocompression and solder bonding have soft metal layers between the substrates. Pressure or heat is applied to bond the layers together [18]. Other groups have used these techniques, and their variations to integrate microfluidics and ICs to develop cell growth tracker [19], impedance sensors [20], cytometry [21], and capacitive sensor [22].

These microfluidic fabrication and bonding techniques are optimized to develop microfluidic devices on ICs, but require sophisticated machines and techniques. This affects the cost of the final system and skill required to develop these sensors. Instead of fabricating the microfluidic device directly on CMOS, some groups have fabricated the devices on a glass slide or

a cover slip and placed it on the CMOS sensor [23] [24]. Although this is an effective technique, sample-sensor separation is incompatible with lensless fluorescence imaging and many chemical sensing methods.

2.3 Project outline

This chapter solves the existing problems with CMOS microfluidic fabrication by proposing heat seal adhesive (HSA) tapes fabrication technique. These tapes will be patterned using a laser cutter, fabricated on CMOS, and sealed with a slab of PDMS. After fabrication on CMOS, the performance of HSA device will be quantified by measuring the pressure, edge uniformity, and surface roughness of the fabricated microfluidic device. Due to the delicate nature of CMOS, quantitative studies will be performed on glass fabricated microfluidic devices and then optimized to test CMOS fabricated devices. The performance of HSA devices will also be compared to other devices.

2.4 Methods

This section outlines the fabrication protocol for developing microfluidic devices on a glass slide and CMOS sensor. Protocols for fabricating HSA, PSA, and PDMS devices are presented in detail in this section.

2.4.1 Fabrication of HSA microfluidic device on a glass substrate

HSA tapes are made up of a polyester layer coated with heat activated adhesive on both sides. These tapes are flexible, translucent, and adhere well to surface such as glass, CMOS, and PDMS. The tapes were purchased from Adhesive research (ARcare 92848) and the schematic of the tape is shown in Figure 1.



Figure 1 Anatomy of the heat seal adhesive tape [25]

The design of the microfluidic device was drawn in AutoCAD and the tape was patterned using a CO₂ laser (Epilog Zing – Model 10000). After cutting, the tape was cleaned by sonication; it was placed in 15% isopropanol for 5 minutes, and in DI water for 5 minutes. The tape was dried using pressurized air and incubated overnight. To reduce the hydrophobicity induced by laser patterning [26], the tape was treated with the UV-ozone cleaning system the next day. Uncured PDMS mixed at 5:1 (v/v) base:curing agent was poured in a dish with a flat base and cured. A slab of PDMS was cut to dimension to make the top layer of the microfluidic device. The slab was then punched with a blunt needle to form ports. Two techniques were tested to bond the tape to the glass slide; direct and indirect adhesive activation. During direct activation, the tapes were laid on the glass slide and placed on a hot plate for 5 seconds. During indirect activation, the tape was placed under a hot air gun for 5 seconds to activate the adhesive and was then laid on the glass slide. Experiments showed no significant difference between the two techniques. After the tape was laid, a punched PDMS slab was placed on top and held down for two seconds. The device was then allowed to cool for a minute.

During the study, it was observed that HSA devices performed well for most imaging applications, but for applications that require high speed imaging or high pressure, the seal strength was not consistently adequate. To overcome this potential pitfall, the HSA devices were reinforced with PDMS. These HSA+PDMS devices demonstrated superior performance when compared to PSA, PDMS, and HSA devices. To fabricate these devices, adhesive on the patterned tapes were activated and laid on the glass substrate. A slab of punched PDMS was placed on top and allowed to cool. Uncured PDMS was then loaded in a syringe and dispensed around the PDMS slab. The slide was placed under a hot air gun for 2 seconds to cure the thin layer of uncured PDMS. Once cured, the PDMS on the edge acted as reinforcements forming a reliable tight seal. Figure 2 shows the fabricated devices.

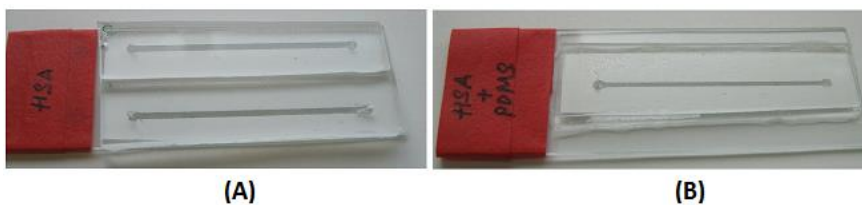


Figure 2 HSA microfluidic device fabricated on a glass substrate (A) HSA device (B) HSA+PDMS device

2.4.2 Fabrication of HSA microfluidic device on CMOS sensor

The protocol to pattern and clean glass based microfluidic devices were followed for CMOS based devices. The cleaned tapes were placed on a punched PDMS slab cut to dimensions. The slab and the tape were placed under a hot air gun for 5 seconds to activate the adhesive. The slab with the tape was then placed directly on the CMOS sensor. The device was held in place for 3 seconds before it was allowed to cool. The adhesive was heat activated before it was placed on the CMOS to prevent sensor damage due to heat and to evenly activate the adhesive. If the

adhesive was activated after placing the tape and PDMS on the CMOS, the heat did not transfer uniformly to the tape through the layer of PDMS.

To make HSA+PDMS devices, an insulin syringe loaded with uncured PDMS was employed. After the device was allowed to cool, small amounts of PDMS was dispensed around the device on the surface of the sensor. The sensor was exposed to a hot air gun for two seconds to cure the PDMS. The fabricated devices are shown in Figure 3.

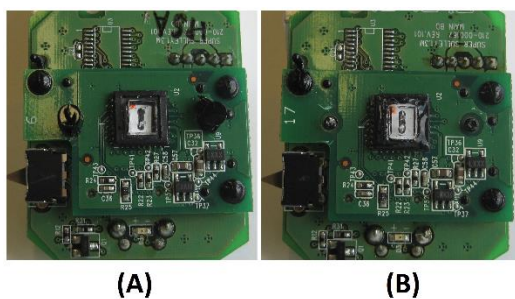


Figure 3 HSA microfluidic device fabricated on a bare CMOS sensor (A) HSA device (B)
HSA+PDMS device

2.4.3 Fabrication of PSA and PDMS microfluidic devices

To compare the performance of the HSA devices with other devices, PSA and PDMS devices were developed. PSA tapes are very similar to HSA tapes with a polyester layer and adhesive. Unlike HSA, the adhesive on these tapes need pressure to be activated. Other groups have used PSA fabrication to make devices on glass, plastic, and paper [26] [27] [28]. PSA devices were selected for comparison due to its similarity to HSA and ease of fabrication. Due to the wide use of PDMS for fabricating microfluidic devices, PDMS devices were also employed for

comparison. The fabrication technique to develop the devices on glass and the protocol used for testing is presented in this section.

While designing the devices for glass fabrication, channels with different widths were designed; the channel width was varied from 0.1mm to 1mm. To make a PSA device on glass, the tape was patterned and cleaned similar to HSA device fabrication. The protective layers on the tape were peeled and carefully placed on a glass slide to prevent air bubbles. A slab of PDMS with punched ports was carefully laid and even pressure was applied to bond the layers together. A similar protocol was followed to develop the devices on the CMOS sensor. The fabricated devices are shown in Figure 4.

PDMS devices fabricated in our lab are generally fabricated by etching a copper plate to create a master. This method is similar to the toner transfer masking technique presented in [29]. The surface and edge variation of the PDMS devices made from masters depends on the surface quality of the master, hence an alternate technique was employed. The design of the microfluidic device was fabricated on a PCB and used as a master. To make the device, uncured PDMS was mixed at 5:1 (v/v) base:curing, poured over the master, and allowed to cure overnight. After the device hardened, it was peeled and punched using a blunt needle to make the input and output ports. Since PDMS does not possess adhesive properties like the tapes, a modification of the stamp and stick technique presented in [18] was employed. A thin layer of uncured PDMS mixed at 5:1 (v/v) base:curing agent was spread on the glass slide. The cured PDMS was placed on this slide and heated on a hot plate for 30 seconds. The heat cures the thin layer of PDMS and bonds the device to the glass slide. Fabricated devices are shown in Figure 4.

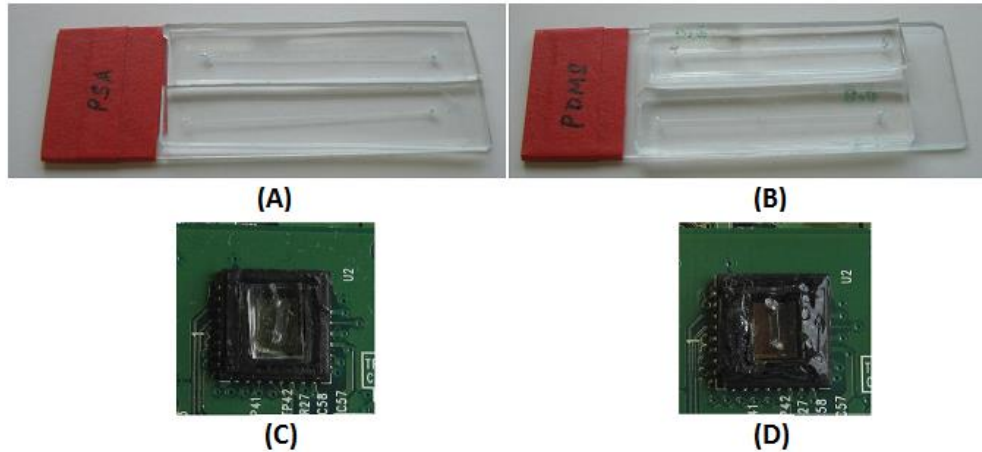


Figure 4 PSA and PDMS microfluidic devices (A) PSA device on a glass substrate (B) PDMS device on a glass substrate (C) PSA device on CMOS (D) PDMS device on CMOS

2.5 Results

This section presents the results from the comparative study of the fabricated devices. The set up for measuring the performance parameters and the protocol for testing is detailed below. The measurement set up were tested on glass slide device before they were employed to test CMOS devices.

2.5.1 Pressure test

Pressure was selected as one of the criteria to compare the devices as it quantifies the strength of the seal. The device should be strong enough to handle sample flow; due to the small feature size of the CMOS microfluidic devices, the speed at which the sample is injected and the pressure applied by the tubing at the ports have a huge effect.

Pressure sensors from omega (PX26-015GV) were purchased and calibrated. For preliminary data, microfluidic devices fabricated on glass slides were employed. A 22 gauge

needle (BD PrecisionGlide) was used to punch the ports and #30 size tubing (Cole Parmer PTFE #30 AWG) was inserted at the ports. The tubing from the input port was attached to an empty syringe, and the tubing from the output port was attached to the pressure sensor. The electrical connections for the sensor were made as mentioned in the user manual. Calibration and measurements were performed at 10 V. Figure 5 shows the pressure measurement set up.

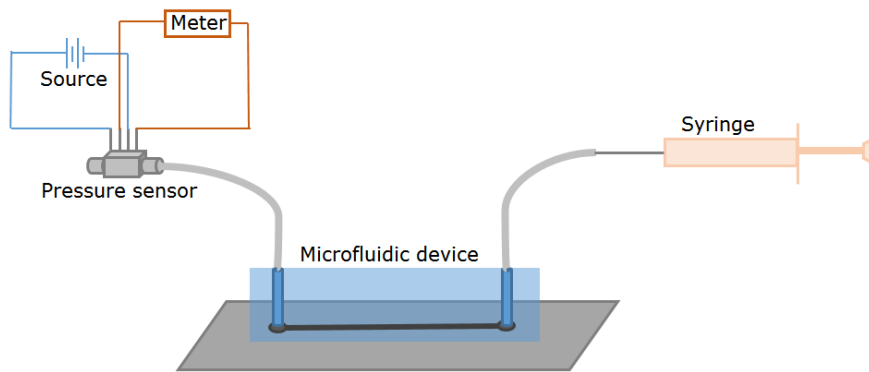


Figure 5 Pressure measurement set-up to quantify the amount of pressure a microfluidic device can withstand

Data from 8 glass fabricated and 4 CMOS fabricated microfluidic devices were collected by injecting a gust of air into the devices. The voltage reading on the multimeter connected to the pressure sensor was recorded. As the air was injected, the pressure inside the device builds up before a leak is formed. The equivalent pressure corresponding to the highest voltage value was determined using the calibration graph.

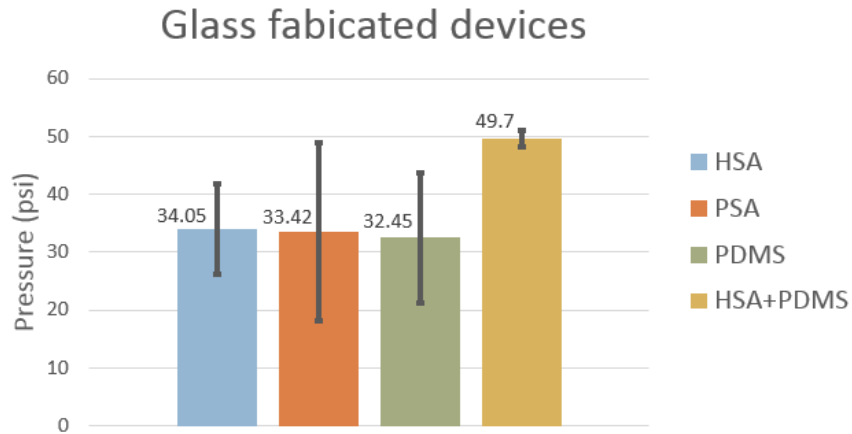


Figure 6 Pressure test for HSA, PSA, PDMS, and HSA+PDMS devices on a glass slide. The columns represent the mean pressure and the error bars represent the standard deviation

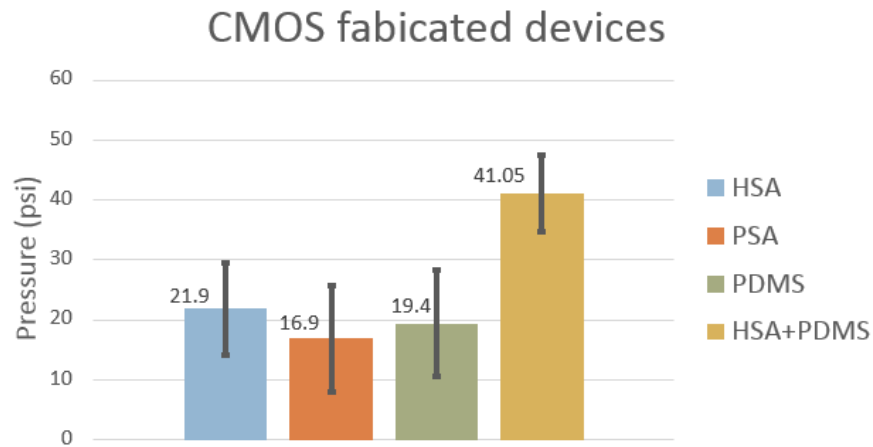


Figure 7 Pressure test for HSA, PSA, PDMS, and HSA+PDMS devices on a CMOS sensor. The columns represent the mean pressure and the error bars represent the standard deviation

From the data, it can be observed that HSA devices perform better than PSA and PDMS devices, with HSA+PDMS devices demonstrating much better performance. The performance of

PSA devices were prone to trapped bubbles between the tape and the glass substrate; devices with trapped air demonstrated lower performance by a noticeable amount.

2.5.2 Surface roughness

Surface roughness on the materials used for fabrication contribute to height variation. The height of the channel is critical for optical applications; if the variation is too high, it might lead to data loss. Hence, to measure the surface roughness, an optical profiler (WYCO NT3300, Veeco Instruments) was employed. To measure PDMS, the surface of a cured microfluidic device was measured. For the tapes, the surface variations before and after the activation of the adhesive did not make a significant difference. The average variation in height on the surface of HSA, PSA, and PDMS was found to be 3.39 μm , 4.26 μm , and 3.35 μm respectively. Since the surface roughness for HSA+PDMS devices depends on the surface roughness of HSA tapes, they were not measured separately. The y axis on the graph represents the height of the material and the standard deviation represents the surface roughness.

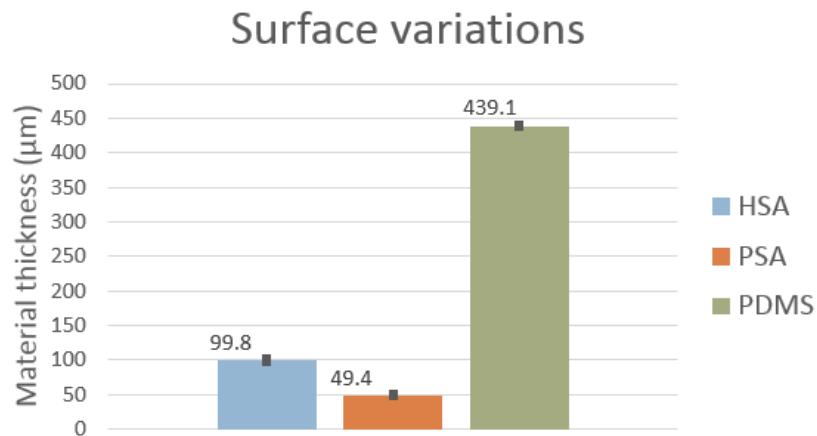


Figure 8 Surface height variation on HSA, PSA, and PDMS. The graph shows the mean and the standard deviation

The variation on the PSA and HSA tapes are defined by the properties of the tape, but the variations on the PDMS depends on the quality of the master used. For applications that require smoother surfaces, the surface uniformity of the masters must be improved. From the data, it can be observed that the variations on the surfaces are not very significant, but on a comparative scale, HSA shows less variation than PSA and matches the performance of PDMS devices.

2.5.3 Edge uniformity

Edge variation is critical in sample flow studies and focusing applications; small variations in the channel, especially on the edges affect the path of the sample. Edges on a microfluidic device act as boundaries, restricting the flow of sample. From our experiments, we observed that the samples flowing close to the edges of the microfluidic device, mimic the variation along the edges. For applications such as sample flow measurements and sample focusing, the quality of the edges play a critical role. During the study, it was observed that the settings on the laser cutter used for patterning the tapes had a huge impact on the quality of the edges. Hence, a range of settings were used for patterning, before picking the ideal settings. The settings on the laser that were modified were power, speed, and number of runs. The power determines the amount of energy the laser uses while making the cut and the speed defines the amount of time the laser spends on one spot. The user manual mentions that making multiple runs with lower settings would make a smoother cut than making one run at high power. The optimum speed and power depends on the properties of material, thickness of the material, and the channel width. We observed that narrower channels required more runs and different settings to make smoother edges. The settings that provided the best edge for PSA and HSA tapes are shown in Table 1.

Device	Speed	Power	Number of runs
PSA Channel width: 0.1-0.4mm	100%	1%	5
PSA Channel width: 0.4mm-1mm	1%	1%	3
HSA Channel width: 0.1-0.4mm	100%	100%	5
HSA Channel width: 0.4mm-1mm	100%	100%	2

Table 1 Speed, power, and run settings on the laser cutter used in patterning the tape for microfluidic fabrication

For devices fabricated on glass slides, images of the edges at different sections on the microfluidic device were captured using a microscope. These images were then analyzed in Matlab to determine the variation. The algorithm used for measuring edge variation is illustrated in Figure 9. The original image was read by the Matlab code and converts the image to gray scale. A canny filter was applied to the image to obtain the edge information. The image was then dilated to connect the discrete points. Boundary conditions were applied on these regions to retain the edge information for analysis; retained boundary are marked as upper and lower boundary lines. A function was then used to fill gaps in the retained edge; the function draws a straight line between discontinuous regions. After a continuous edge was retained, line of best fit was drawn and the root mean square error was calculated.

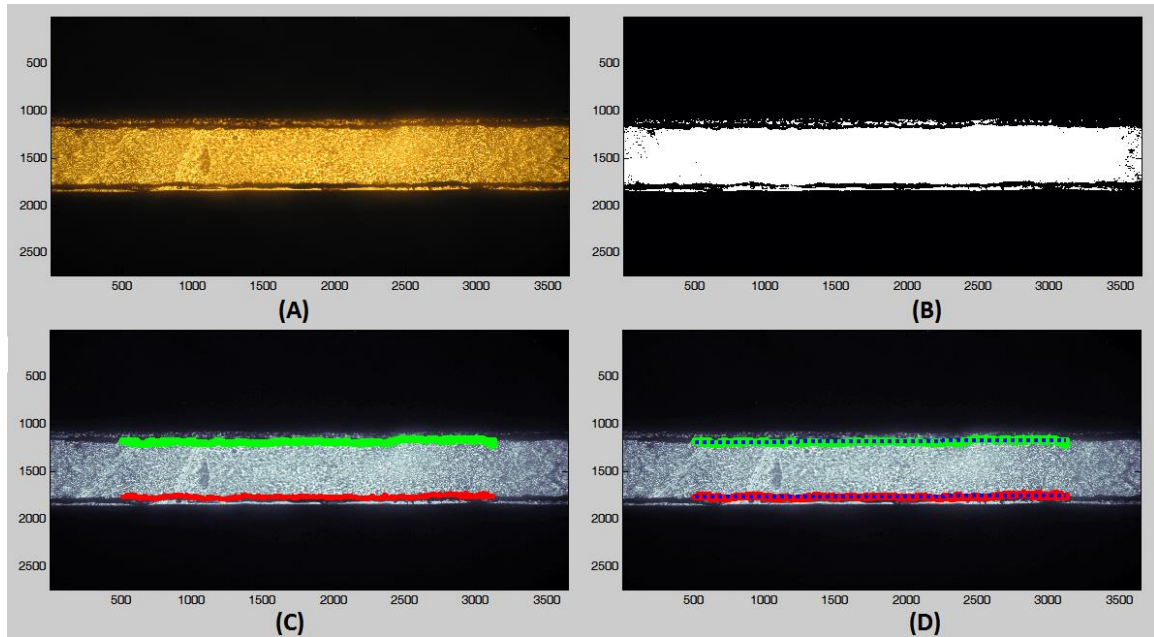


Figure 9 Stages in the Matlab code for quantifying edge variation. (A) Original image (B) Image after edge detection (C) Identifying boundaries (D) Boundary with best fit line

During fabrication, it was observed that channels made of PSA showed high variations. This was due to the pressure applied during sealing the device; when pressure was applied, the adhesive on the edges was forced into the channels causing uneven edges with sharp transitions. Cleaning a PSA device was also challenging as the adhesive trapped small dust particles and debris. Quantification of the variation using the matlab code supported our hypothesis; PSA devices showed maximum variation along the edges. Performance of HSA devices is comparable to PDMS devices. The root mean square error of the variation along the edges is summarized in 19Figure 10 and Figure 11. Since the edges of the HSA+PDMS devices are formed by HSA tapes, those devices were not measured.

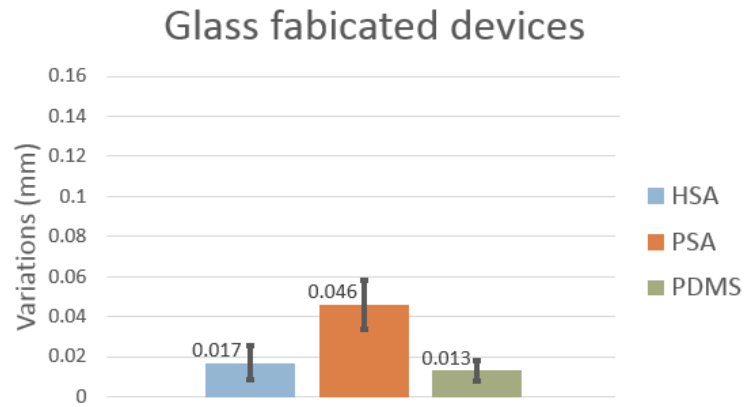


Figure 10 Edge variations in glass fabricated devices

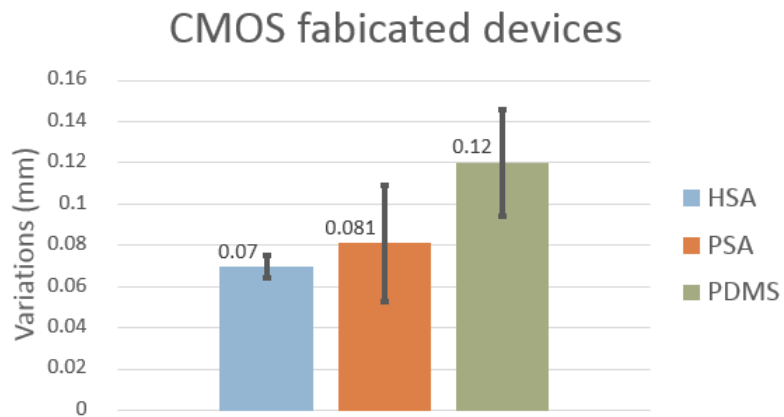


Figure 11 Edge variations in CMOS fabricated devices

The graphs show that CMOS fabricated devices show more variations in comparison with glass fabricated devices. This is due to the uneven surface of the CMOS sensor; minor variations induced by the surface also contribute to the variations measured by the code. Among the three devices, HSA showed the lowest variations both on glass and CMOS substrates.

2.6 Conclusions

HSA fabricated devices show improved performance while reducing cost and fabrication time. Fabrication of microfluidic devices using HSA tapes and reinforced HSA+PDMS devices would offer better results in applications such as hydrodynamic focusing, flow cytometry, pinched flow fractionalization, micro total analysis systems, and hydrodynamic rectification. The inert chemical properties of the tape makes it ideal for sample delivery and handling in chemical, biological, and environmental sensors.

CHAPTER 3

ON-SENSOR FLUORESCENCE IMAGING DEVICE FOR SCREENING BLOOD

Blood performs many important tasks such as transportation of oxygen to organs, attacking foreign cells, protecting the body from infection by generating antibodies, and regulating the body temperature to name a few [30]. Blood also contains a lot of information about the individual's health; a complete blood count (CBC) is the most common test performed at hospitals. While performing a CBC, the cell count, morphology, inclusions, cell size, and cell shape of blood cells are studied. Changes in these properties are associated with various disease such as infections, bleeding and clotting disorders, and anemia to name a few. There are other specific blood tests that can screen an array of disease such as hemophilia, diabetes, cancers, leukemia, lymphoma, myeloma, Ebola, HIV, and hepatitis. Blood is also studied for health monitoring as it sheds light on cholesterol levels, liver function, kidney function, oxygen levels, toxicity levels, and other important markers for general health [31]. The recognition of blood as a corner stone to diagnosis led to the development of many specialized medical instruments.

To optically analyze blood, the cells have to be stained; cells are transparent and need stains to improve contrast during imaging. Normal stains are used to merely highlight sections of the cells, such as the nuclei, cell membrane, and mitochondria. Fluorescent stains are more specific and sensitive than normal stains; they stain the components within the cell by chemically binding to the target. They also provide better contrast during imaging due to the presence of fluorescent nanoparticles. These nanoparticles are known as fluorophores; they absorb light at a specific wavelength and emit light of a longer wavelength. This phenomenon was first observed

in 1852 by Sir Gabriel Stokes and numerous dyes are commercially available to stain various proteins present in cells [32].

Fluorescence imaging has proved to be a useful clinical tool, leading to the development of imaging equipment such as fluorescence microscopes and flow cytometers. These equipment screen a range of diseases including blood related disorders, cancers, and AIDS. Microscopes have been an indispensable equipment in diagnosis by providing both qualitative and quantitative information about the sample. The downside of microscopes is manual screening; the reliability of this method depends on the experience of the clinician or the pathologist. Flow cytometers are automated devices that also provide quantitative and qualitative information, making them the state-of-the-art technique to screen for human immunodeficiency virus (HIV). The drawback of these devices is the costs associated with the device; commercial flow cytometers cost \$35,000 or more and have a maintenance costs of \$6000 per year [33]. The other drawback of this device is clogging; analysis is performed only on one cell at a time, hence the size of the aperture must be small. The device can handle cells up to 100 μm , which is wider than most cells. The problem arises when two or more cells are lumped together or when an abnormal cell is being analyzed. Cancer cells and other unhealthy cells usually tend to be larger than healthy cells, clogging the system during analysis.

3.1 Problem statement

The cost, fragility, and maintenance of existing fluorescence imaging devices limits their use to central laboratories. This chapter demonstrates that lensless fluorescence imaging can also offer qualitative and quantitative information about the sample. Capability of the device to

analyze more than one sample at a time and techniques to improve throughput is also presented in this study.

3.2 Literature review

To analyze sample with a flow cytometer, the sample must be stained with fluorescent dyes using direct labeling or indirect labeling methods [34]. Once stained, it is placed in the device for analysis. The device employs hydrodynamic focusing to channel the cells into a thin stream. The cells are then exposed to a laser, one cell at a time, causing the stained sample to emit fluorescence. This emission is recorded using photomultiplier tubes and photodiodes. The device records the front, back, and side scatter from the sample. Using all this information, the flow cytometer can provide cell count, classify cell types, and chemical expression without having to study the morphology of the cells [35].

To overcome the drawbacks of conventional flow cytometers, some groups have proposed techniques to miniaturize the device; currently there are two approaches. The first approach employs the same working principle of flow cytometer by focusing the sample into a single file. Instead of using the conventional set-up, the functionality is implemented on a microfluidic chip [36] [37]. This technique still needs an external imaging device such as a fluorescence microscope to perform sample analysis. The second approach employs an array of sensing elements to perform lensless imaging. In this approach, the sample is allowed to flow laterally, increasing cell analysis rate. This technique has been used to analyze sample using white light imaging, where the shadow of the sample is studied to provide information such as sample count [38] and movement [39]. The limitation of these techniques is their inability to perform fluorescence imaging. The specificity and advantages that fluorescence imaging has to offer

cannot be exploited by these devices. This drawback reduces the clinical significance of these miniaturized devices. Existing miniaturized imaging systems that perform lensless fluorescence imaging employ techniques such as total internal reflection [40], time-domain excitation separation using high speed pixels [41], spin coated filters [42], and fiber optic phase plate with fixed sample-sensor separation [43].

In lensless imaging, the sample is directly placed on the imager to collect optical information. If the object is small and close enough, then lenses are not required to focus the image on the sensor. This is the principle behind lensless imaging. This type of imaging has been possible only in the recent past, due to reduction in CMOS feature size. The lack of lenses, reduces the effective imaging area to a few millimeters above the imager, making this technique ideal for biological samples. A representation of lensless imaging is shown in Figure 12, the checked pattern represent the pixels and the red disks represent red blood cells. Figure 13 shows how the signal to noise ratio decreases as the sample-sensor separation increases during fluorescence imaging.

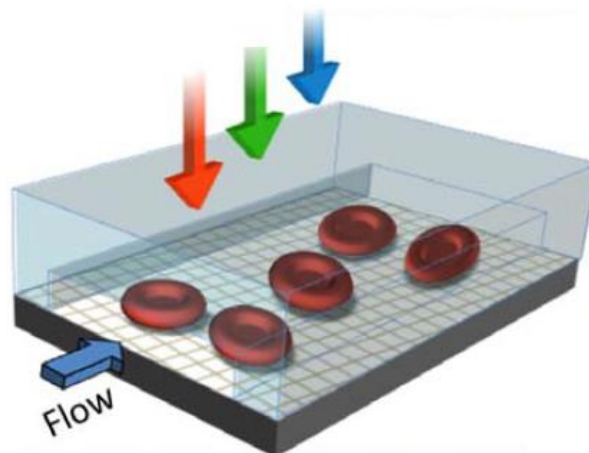


Figure 12 Illustration of lensless imaging [44]

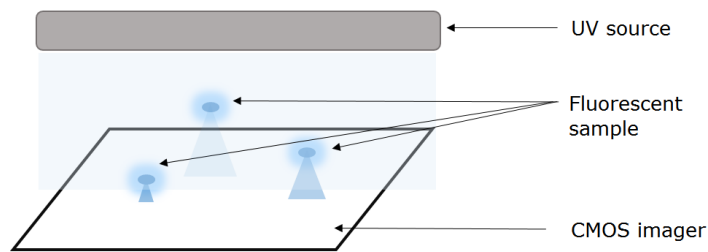


Figure 13 Effect of sample sensor separation on lensless fluorescence imaging

3.3 Project outline

The drawbacks of existing imaging devices can be overcome by developing a lensless imaging device capable of fluorescence imaging. The proposed device consists of an imager and a single light source. To offer high throughput, the setup will be designed to analyze flowing sample with varying sample-sensor separations. A calibration graph will be generated to quantify the variation in signal strength due to height. The capability of the device to track the sample movement will also be presented. The performance of the device with fluorescence beads and cells stained with fluorescent dye will also be demonstrated.

3.4 Methods

CMOS imager from a Logitech (QuickCam Communicate MP S5500) webcam was employed to demonstrate lensless imaging. The imager was water proofed before exposing the surface to biological samples. Generation of a calibration graph is critical to deliver reliable data while quantifying signal strength as it accounts for the signal reduction due to sample sensor separation. This section details the generation of the calibration graph and the set up to perform lensless imaging.

3.4.1 Device calibration

Calibration is achieved in two steps. In the first step, the sample was suspended at random but fixed heights. In the next step, the width of the fluorescence signal and the height of the sample was measured. This was performed multiple times to populate the graph shown below. After the calibration graph was generated, it was used as a reference to quantify the signal strength during imaging.

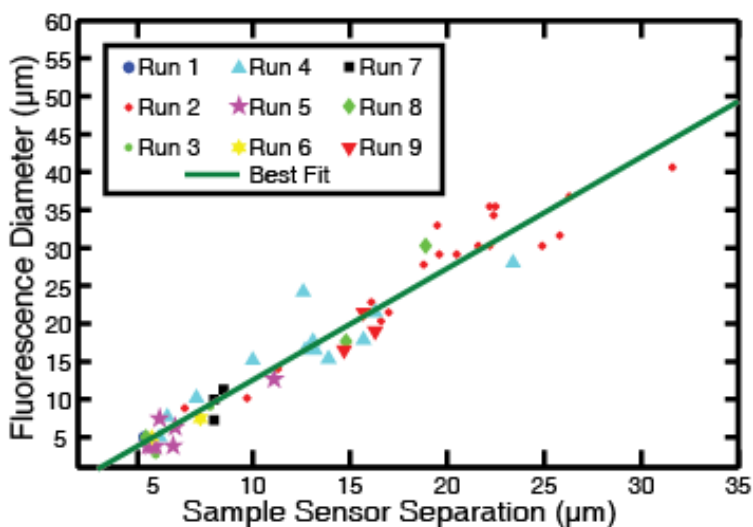


Figure 14 Calibration graph that relates the signal strength and the height of the sample

[45]

3.4.2 Lensless fluorescence imaging

There are three main steps involved in developing a lensless imaging system: imager preparation, microfluidic fabrication, and validation. To prepare the imager, the casing and the protective glass were removed to expose the bare CMOS imager. To avoid exposing the circuits to biological sample, superglue was dispensed on the bond wires to waterproof them. The imager

was left undisturbed overnight before fabricating the microfluidic device. A pressure sensitive tape (PSA) fabrication technique was employed for initial experiments; after the advantages of HSA devices were quantified, HSA microfluidic devices were then employed. Microfluidic fabrication techniques mentioned in the previous chapter was employed to develop PSA devices on CMOS. The fabricated device used for this study is shown in Figure 15.

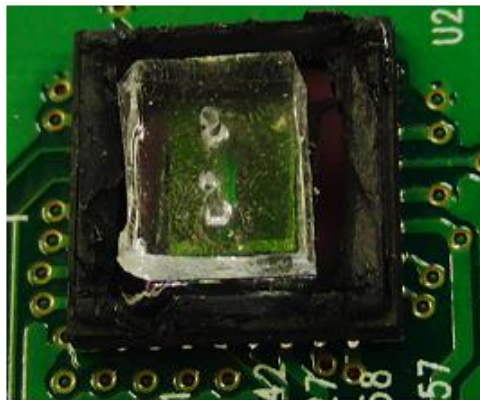


Figure 15 PSA microfluidic device fabricated on a bare CMOS sensor for lensless imaging

[46]

The capability of this system was validated by imaging two types of samples: fluorescence beads and cells stained with fluorescent dyes. Considering the fragility of live cells, the imaging device was first tested with commercially available fluorescent beads (Spherotech FP-10045-2); these beads are used to calibrate clinical flow cytometers. During imaging, 1 μL of the original solution was mixed with 500 μL of DI water to make the working solution. To prepare biological sample stained with fluorescence dyes, RAW 264.7 cells from ATCC were grown on fibronectin treated glass slides and incubated overnight. Quantum dots from Invitrogen (Q25011MP) were mixed and incubated with the cells for 3 hours. Once the cells were stained, they were detached using trypsin and centrifuged. The cells were then harvested and mixed in PBS.

The imaging setup consisted of a CMOS fabricated microfluidic device, syringe pump, and a UV source; the complete set up is shown in Figure 16. Tubing with a diameter of 1mm was inserted at the input and output ports to carry the sample. Due to the flexible nature of PDMS, the polymer automatically forms a tight seal around the tubing. Tubing from one port was connected to a syringe pump containing the sample. Tubing from other end of the microfluidic device was attached to a microcentrifuge tube to collect the imaged sample. During white light imaging, the environmental light was used to illuminate the sample and the shadow casted by the sample was recorded for analysis. For fluorescence imaging, the sample was excited with a UV source. For this experiment, a hand held UV source was employed. A video of the sample flowing through the device was recorded and the frames were analyzed in Matlab.



Figure 16 Imaging set up to perform lensless imaging [46]

After the video of the sample flowing through the microfluidic device has been recorded, the Matlab code splits the video into individual frames. To improve processing speed and save space, one in every five frames are analyzed. The following image processing is performed on each

frame to detect the beads in the frames. A threshold function is applied to the first frame to retain the beads and remove the background. The pixel location of the center of the retained beads is saved in a matrix. A small bounding box is drawn around the retained point to include the bead. A 2D gaussian fit is performed to measure the diameter of the fluorescence emission. This data is collected from all retained frames. To track the sample across frames, boundary conditions are set in Matlab based on the sample injection speed. The pixel values of the center of the bead from frame 'n' is used to define a bounding box for frame 'n+1'. The location of the bead inside the bounding box is saved. The bounding box is used to find the location of the beads from the input port to the output port.

3.5 Results

During imaging, sample was injected into the PSA device at the rate of 5 $\mu\text{L}/\text{min}$. to perform UV imaging, the sample was excited with a UV source and Consecutive frames of the video captured by Matlab while the sample was allowed to flow is shown in Figure 17.

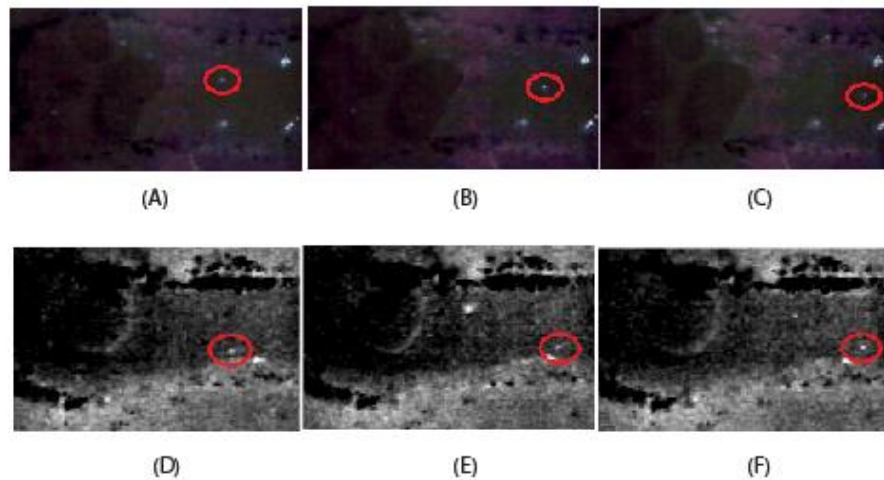


Figure 17 Consecutive frames of sample flowing inside a PSA microfluidic device. (A-C) fluorescent beads (D-F) cells stained with fluorescent dyes [45]

3.5.1 Results with flow applications

Imaging techniques such as streak imaging and particle image velocimetry provide information on sample flow but offer poor height resolution. These techniques also require an elaborate imaging set up for recording the sample. By employing the proposed imaging setup, sample movement can be determined by recording a video of the sample flowing on the imager. Matlab code can detect and track the movement of sample across frames. In the example shown below, the code tracks the movement of a fluorescent beads inside a HSA microfluidic device. The solid black lines represent the walls of the microfluidic device and the dashed black lines are the input and output ports. The solid red line with markers represents the path of the fluorescent beads.

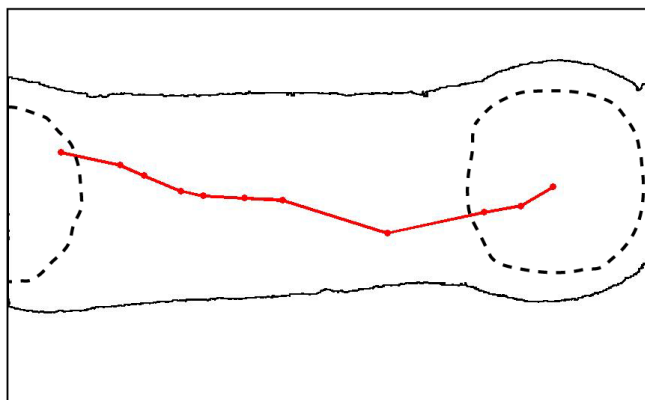


Figure 18 Sample tracking using lensless fluorescence imaging device and HSA microfluidic device

3.6 Conclusions

The capability of the proposed imaging device to perform fluorescence imaging creates numerous clinical applications. The ability to offer both quantitative and qualitative information has diagnostic significance as it can be used to classify cell types. Fluorescence dyes used to stain

the cells offers specificity required to detect organisms such as virus and proteins present in the sample.

CHAPTER 4

SINGLE USE LOW COST ASSAY FOR HEPATITIS C SCREENING

Hepatitis C is a disease that affects the liver; this disease is caused by the hepatitis C virus (HCV) and it primarily spreads by blood-to-blood contact. The symptoms of the disease are hardly noticeable and infected individuals can live up to years completely unaware of the infection. Over time the disease causes liver damage, liver tissue scarring, liver cancer, and eventually results in death [47]. In the US about 3.7 million individuals are infected and 2.8 million (75%) are undiagnosed; globally, the total number infected is about 170 million [48]. The complexity in handling this disease has many dimensions; some of the issues are discussed here.

There are currently no vaccinations available for HCV, and the success of treatment depends on how early the disease is diagnosed [49]. Due to the way in which the disease manifests itself, the presence of the virus is detected usually after the disease has progressed. This has a huge impact on the treatment costs and recovery [50]. The other factor contributing to the high undiagnosed percentage is the high risk population for this disease; this population mainly consists of injection drug users, prisoners, and individuals at homeless shelters. A huge fraction of the infected population, especially the high risk population suffer from serious economic problems preventing them from getting themselves tested for HCV. More than 75% of the infected population are baby boomers; people born during 1945-1965. The reason for this is due to the high prevalence of HCV infection during that period. HCV was identified only in 1988 and tests were developed only in 1992. Blood transfusions, organ transplantation, and lack of awareness about this disease before this period contributed to the steady increase in the number of infected cases [51]. The percentage of the infected population who are unaware of their infection, continue to spread the disease making this a growing problem [52].

At hospitals and clinics, screening is conducted by performing two tests: serologic assay and molecular assay. The serologic assay, looks for the presence of HCV antibody in the blood serum collected from the individual. This indicates that the individual's immune system is actively fighting the virus. The molecular assay, looks for the presence of virus in blood; this test is more sensitive and provides more information on the disease. The results of both tests are critical for proper diagnosis [53], but taking cost and convenience into account, the centers for disease control and prevention (CDC) recommends the serologic assay as the primary test [54].

To screen the high risk population, it is critical to be able to perform screening in the field. There are currently two approaches to field screening: sample collection for conventional screening and rapid testing. In the first approach, a phlebotomist collects blood sample for the serologic assay, and sends the sample to the hospital or clinic. With the result from this test, the phlebotomist makes another visit to discuss the results and collect blood sample for the molecular assay. The sample is then sent to the hospital and with the results, the phlebotomist makes a final visit to discuss the complete results. With every visit the phlebotomists makes, following up with individuals becomes tougher, especially among the high risk population consisting of homeless people. The other problem is the turnaround time and cost; including transportation, this approach has higher associated costs than screening at hospitals. The second field testing approach is to employ a rapid test; these tests are commercially available HCV screening device that can be used in the field, produce results within half hour, and costs less than conventional screening. The downside of these rapid tests is its ability to perform only the serologic assay. The serologic assay can detect the presence of the disease, with exceptions; if the infection was acquired in the past six months or if the individual has a compromised immune system, this test

will not be able to detect the presence of the disease [54]. Immunosuppression is common among individuals infected with HIV and immune system disorders. According to CDC, 25% of this population (0.3 million) is co-infected with HCV; this number represents only a fraction of population that the serologic assay cannot detect [55].

4.1 Problem statement

Lack of resources, accessibility issues, and disease manifestation have been the main obstacles in reducing the number of undiagnosed individuals. A low cost, high speed, field test capable of performing complete screening by detecting antibodies, detecting the presence of virus, and classifying the virus subtype would be an ideal solution to the existing problems. This chapter demonstrates the techniques that can be used to develop a complete rapid test for hepatitis C.

4.2 Literature review

Enzyme-Linked ImmunoSorbent Assay (ELISA) and immunoblot tests are commonly performed for serologic testing at hospitals. ELISA requires a pretreated cell culture plate that has affinity toward the antibodies being screened. The antibody-antigen binding induces a colorimetric reaction, and the change in color is detected using the plate reader. Optical plate readers are equipped with monochromators, diodes, detectors, and optics to quantify the outcome of the test. Field devices such as the OraQuick HCV rapid test performs serologic assays using similar binding techniques for detection. Unlike ELISA, this test uses indirect lateral flow immunoassays [56]. A list of rapid tests that can perform serologic assay is presented in Shivkumar *et.al.* [52].

Molecular testing provides quantitative results by detecting the amount of virus present in blood. It also provides information on genotyping; HCV can be classified into at least 6 major sub types. The subtype information is critical in deciding the treatment plan for the individual [53]. Manual or semi-automated reverse transcriptase polymerase chain reaction (RT-PCR) is used for performing this test. All cells, including viruses have a nucleus with Deoxyribonucleic acid (DNA); the DNA contains the genetic information of the virus. Molecular assays detect the presence of the virus by identifying this genetic information. The concentration of the virus in blood is as low as 10-50 IU/ml, hence the amount of virus has to be amplified for detection. The RT-PCR achieves amplification by binding primers to generate copies of the original DNA sequence [57].

Tang *et.al* have developed a HCV screening device that can not only perform serologic assay by detecting the presence of HCV antibody in blood, but can also classify the subtypes of the virus. The proposed device is an immunosensor array that simultaneously detects the antibodies within 5 minutes. Although the chemistry for the test is carried out on the sensor, an electrochemical analyzer is required for performing the voltammetry analysis limiting the use of this sensor to a laboratory setting [58].

Electrochemical measurements for biosensing can be performed using many techniques such as square wave, cyclic, differential pulse measurements, and electrochemical impedance spectroscopy (EIS). Among them, EIS has the lowest detection limit and can be used to detect various biomolecules [59] [60]. EIS is a label free biomolecule detection technique that measures the changes in impedance for detection. This technique employs electrodes functionalized with molecules that have affinity for the target molecules. As the binding occurs, the changes in surface

impedance is measured. With this technique, it is possible to monitor the changes in real time. In spite of these advantages, the challenges associated with EIS such as bulky instrumentation and expensive bench-top systems, limit the use of this technique. Some groups have developed fully integrated biosensors on CMOS [60] that can perform EIS, but the costs associated with fabrication increases the cost of the device. To reduce the cost and for ease of fabrication, other groups have miniaturized the sensor by fabricating the electrodes on a printed circuit board [59] [61]. The downside of these systems is the need for a lab based electrochemical equipment to conduct the test.

4.3 Project outline

The requirements for developing a screening device for this work will be derived from a human factor study conducted to observe conventional field testing practices. Observations and findings from the study will be used as inputs during system integration to make the device user friendly.

To demonstrate feasibility of the screening device, a prototype that can detect the presence of biological sample will be developed. A PCB consisting of electronics to perform EIS will conduct the tests and the data will be sent to a computer via USB cable. A Matlab code will analyze the data and display the outcomes of the test. A microfluidic device on the printed circuit board will channel the sample to the functionalized gold electrodes where the electrochemical reaction will occur. This chapter will discuss the following aspects of the proposed system: findings from the human factor study, design of the electrodes, protocols to functionalize the electrodes, PCB design, microfluidic fabrication, microcontroller and Matlab code, and results from the device.

4.4 Methods

Serologic assays are capable of detecting the antibody and the virus in the sample. Before PCRs were widely available, serotyping was performed for antibody and virus detection. A study comparing serotyping techniques with genotyping techniques show a high correlation of 94% [62]. The main drawback of conventional serologic assay is the detection; colorimetric readout requires an optical readout machine that detects the enzyme activity in the assay. This work borrows the chemistry from ELISA based testing and uses electronic detection instead of optical detection.

The working principle of the device is binding the target molecule from the solution to the functionalized electrodes on the PCB. This binding will be proportional to the change in the impedance of the electrodes. By measuring the impedance, quantitative information on the target molecule can be obtained. By functionalizing the electrodes with different proteins, tests for HCV antibody and the virus can be designed.

4.4.1. Human factor study

Commercially available HCV rapid screening tests, OraQuick was employed during the human factor study [56]. This device can perform the antibody tests and produce results within 20-40 minutes. The motive behind this study was to observe the steps involved in screening, time taken to perform these steps, and determine the familiarity of technology among subjects. The observations were then used as an input to design the screening device. The study was performed at two performance sites: Hampshire county jail, and at a Samaritan inn in Westfield, MA. A

protocol for the human factor study was submitted to the IRB and approved before the study was performed. A CLIA waiver was also obtained for using OraQuick HCV for screening purposes.

Mobile screening of HCV has certain procedures and policies that has to be followed; the complete list is detailed in Zucker *et.al* [63]. The individuals being screened are required to fill out a risk factor assessment form and past medical history assessment form as a part of routine screening. Before screening, the purpose of the human factor study was explained to individuals and if they were willing to take part, they were asked to sign the consent form and fill out the technology questionnaire. To make the data collection anonymous, a barcode was associated with every subject. The barcode was place on every page of the paper work. Before collecting the blood sample from a finger prick, the finger was sanitized with an alcohol wipe. The first drop of blood was discarded and the next drop was collected using a scoop. The blood was then mixed with the buffer and the test device was inserted into the buffer. A timer was set for twenty minutes to indicate when to check the results.

While screening at the Hampshire county jail, the HCV screening booth was one among 15 booths set up in the facility. Inmates had about 20-30 minutes to visit any booth in the camp. To save time, they were asked to fill out the paper work the night before the screening. At the booth, the subjects read and signed the consent forms before being screened. They were given basic counselling about the disease and on how they can reduce the risk of acquiring the disease. Data from a total of 28 subjects were collected from both sites. The graph shown below illustrates the average time taken each step. The steps mentioned in the graph correspond to the following. Step1: Time taken to fill out all paper work including medical history, risk assessment, consent form, and the technology questionnaire

Step2: Setup time including time taken to prepare the kit for sample collection and collecting blood sample

Step3: Counselling after sample collection

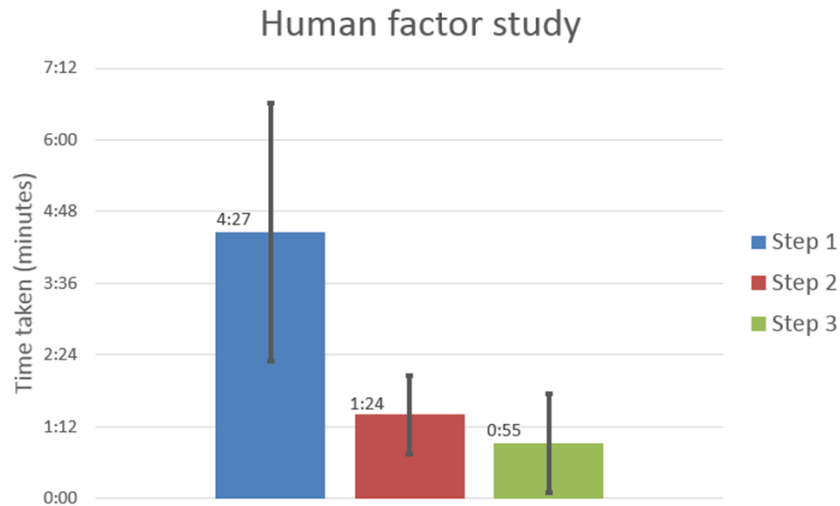


Figure 19 Data collected from the human factor study. Columns represent the mean and error bars represent standard deviation for each step in screening [64]

The standard deviation is large because of the following reasons: at the prison, since the inmates were asked to fill out paper work the night before screening, data for step 1 was collected by asking them how long the paper work took. At the Samaritan inn, there were no time constraints and the subjects spent more time in step 1 and step 3.

The technology survey asked the subjects to answer the following questions: if they have used smart phones, do they use text messaging services, if they have an email account. From the data collected, 20 out of 28 have used smart phones in the past three years, 19 out of 28 use text messages, and 21 out of 28 have email accounts. Only 5 out of the 28 answered no to all three questions.

Based on the observations and conversation with the personal involved in screening, some key observations were made. An average of 70% of the total screening time is spent in paper work. Familiarity with technology among the focus group can be used to our benefit to replace paper work; all forms and personal information can be collected electronically.

Most of the time spent on step 2 were to set up the kit for sample collection; the kit contains a loop for sample collection, a container for the buffer, a stand to hold the container, and the test device itself. They are individually wrapped and have to be opened right before using them to reduce chances of contamination. With the time constraint at the county jail, two trained personnel was required to set up and collect samples respectively. A system that has a simple user interface would reduce the time spent in this step.

Since the results of the rapid test employed in this study had to be read out manually, a nurse had to set a timer, match the barcodes with the sample containers, and manually record the results for each subject.

Counselling is a critical step in screening, as it educates the individuals about the disease. Apart from individual counselling, email, text messages, and other technology aided modes can be employed to make this more effective. Technology could also help with following up with individuals and providing them information regarding screening centers and health camps.

From these findings, the following inputs for the proposed system were identified. The device has to possess a simple interface to expose the blood sample to the electrodes. The

screening must be affordable and take less than 10 minutes. Screening must be completely automated and reliable.

4.4.2. Electrode design

Many different geometries and materials have been studied for electrochemical measurements. Conventional measurements employ 3-electrode systems consisting of a working, reference, and counter electrodes made of gold, platinum, silver, or silver chloride. For our measurements, we employed gold interdigitated electrode due to its increased sensitivity and signal to noise ratio [65]. Interdigitated electrodes have also led to the use of two-electrode systems. Min et.al compared the performance of gold and platinum by studying the signal-to-noise ratio, and overall signal magnitude and concluded that gold had a superior performance [66]. Coating gold on copper wires using electroless techniques is an established protocol in PCB manufacturing [67]. Figure 20 shows the electrode pattern used for this device. The width and the spacing for the electrodes were chosen to optimize the electric field above the electrodes during measurements [68]. The width of the fingers and the spacing between the fingers were designed to be 0.15 mm on both topologies. The small electrodes were designed to be 3 mm x 3 mm and the large electrodes were designed to be 6 mm x 6 mm.

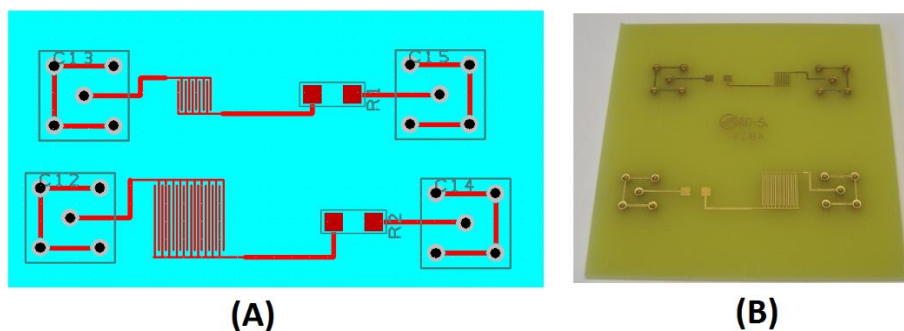


Figure 20 Interdigitated electrodes (A) PCB design (B) Fabricated electrodes

4.4.3. Functionalization protocol

In order to perform EIS, the electrodes must be functionalized to perform affinity-based sensing. To prove that the proposed device can be used for screening, detection of +36 green fluorescence protein (GFP) [69] [70] was demonstrated with this device. To detect the protein, it has to bind to the surface of the electrode; since the protein does not have affinity toward gold, a thiol group was used to induce binding. The illustration of protein binding to the gold is shown in Figure 21.

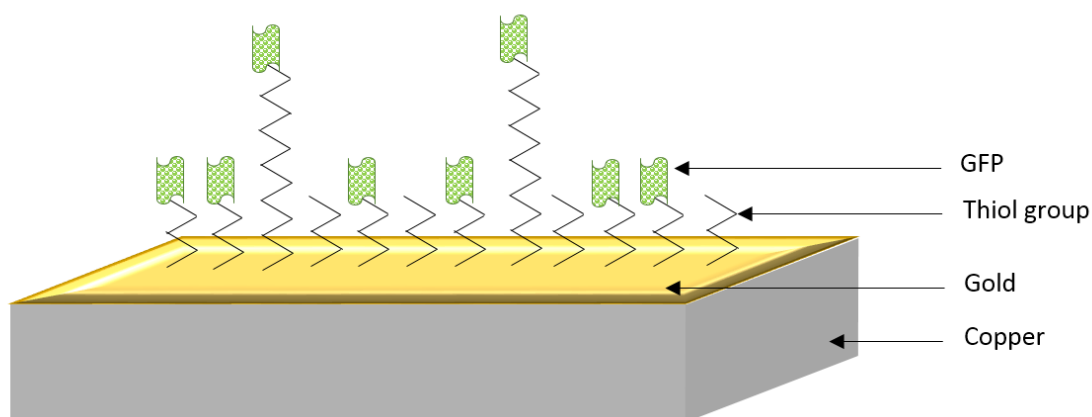


Figure 21 Illustration of gold electrodes with self-assembled monolayer and green fluorescent protein

To form a thiol group on the gold, a self-assembled monolayer (SAM) of 3-Mercaptopropionic acid (3-MPA) and 11-Mercaptoundecanoic acid (11-MUA) was formed. For this study, a 10mM of 3-MPA and 11-MUA were prepared in absolute ethanol. The gold electrodes were cleaned and immersed in 3-MPA and 11-MUA mixed at a 10:1 ratio. After 20 hours of incubation in room temperature, the electrodes were rinsed in ethanol and DI water. A working solution of 3 μ M of the +36 GFP in Phosphate-buffered saline (PBS) was prepared and exposed to

the electrodes for 30 minutes. The electrodes were then washed with PBS to remove unbound protein.

A mixture of thiol groups with different lengths was selected as it demonstrated better surface coverage compared to homogenous thiol groups [71]. During incubation, the thiol group self assembles on the gold surface forming a uniform monolayer; the SH group binds to the gold exposing the carboxyl group. When exposed to the GFP, the protein binds to the exposed carboxyl group.

4.4.4. PCB design

The printed circuit board houses the electrodes, conduct the test, collects the data, and sends it to a computer for analysis. To perform EIS, the electrodes must be fed with a sine wave and swept over a wide range of frequencies. In order to quantify the surface chemistry on the electrodes, the output and the input signals of the electrodes must be measured and compared. This section outlines the working principle of the device.

The main components on the board are the waveform generator chip and the microcontroller. The waveform generator chip (AD5932) from Digikey consists of programmable registers that define the start frequency, frequency increment, and number of increments. The registers were programmed to generate a sine wave output of 500 mV from 100 Hz to 10 kHz. After the registers were written, a pin on the chip had to be pulsed to initiate waveform generation. The pin was pulsed to increase the frequency; each increment increased the frequency by 100 Hz. The microcontroller (PIC32MX795F512L) with bootloader was employed in this study. The PCB was designed with a USB port to facilitate serial communication with the

computer. The microcontroller was programmed to write the registers, provide supply, and clock to the waveform generator chip. The generated sine wave was sent to the electrodes; the input and the output signal of the electrodes are then sent back to the microcontroller. The microcontroller digitizes the signals with the aid of the 10bit ADC and sends the data to the computer via serial interface.

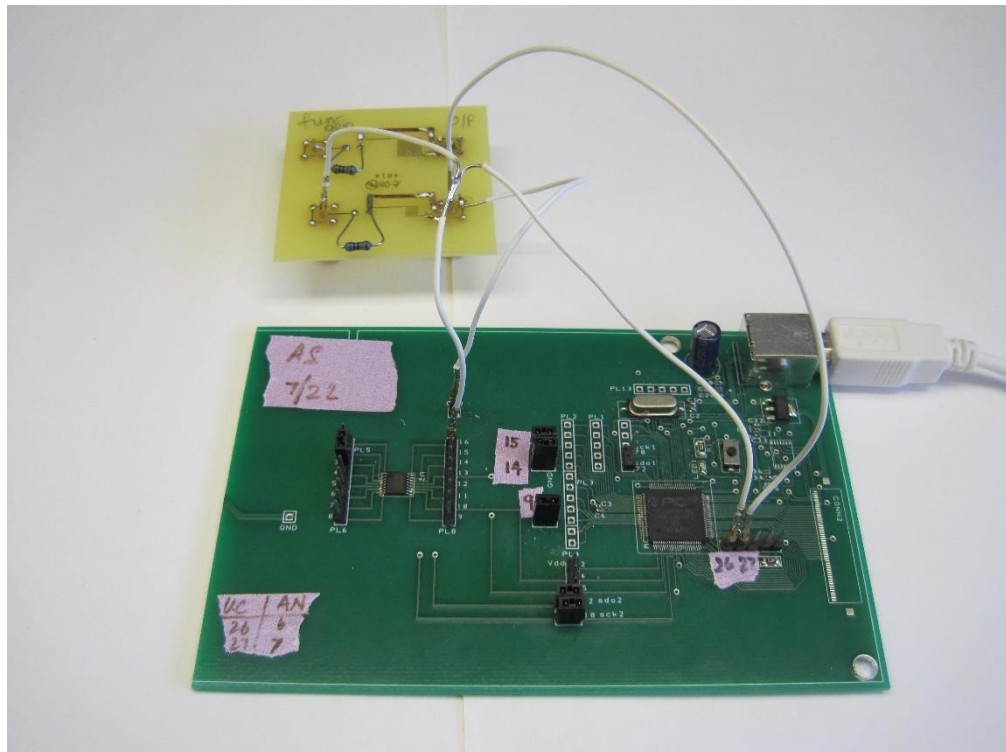


Figure 22 Printed circuit board to conduct electrochemical impedance spectroscopy

The components on the electrode PCB form an impedance divider with the resistor on top and the electrodes in the bottom; the topology is shown in the illustration below. The amplitude of the output sine wave changes depending on the impedance of the electrodes. From initial experiments, a resistance value of $1\text{k}\Omega$ was found to be optimal. The main board consisting of the chips and the electrodes board is shown in Figure 23.

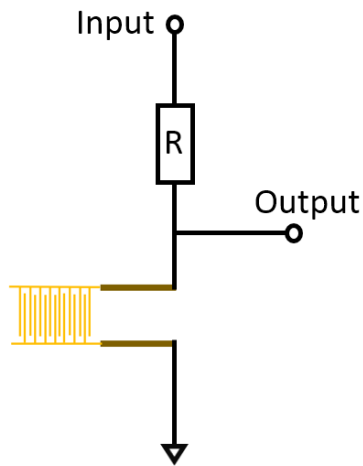


Figure 23 Topology used for measuring impedance change in electrodes

4.4.5. Microfluidic fabrication

The microfluidic device helps to contain the sample directly on top of the electrodes during the test. From the human factor study, it was evident that using sample collection loops and other apparatus increases screening time and effort. Designing a microfluidic device with a wide open port enables the sample to be directly placed on the board. For this application, a simple PSA based microfluidic device would suffice. The fabricated device is shown in Figure 24; blue food color was injected in the microfluidic device to demonstrate functionality. The input port is where the blood from a finger prick will be placed. The sample automatically flows into the electrode region directly on top of the electrodes. The narrow channels offers a high resistance path to the output port; this region ensures that the sample flows into the electrode region and stays on the electrodes during while EIS is conducted.

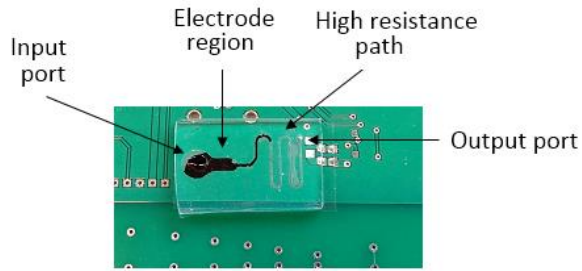


Figure 24 Microfluidic device on PCB for sample containment

4.4.6. Microcontroller and Matlab code

The microcontroller code is loaded on the PIC32 and it runs every time the board is powered. The Matlab code initiates the data transfer from the microcontroller and logs the data for every frequency. The Matlab code then calculates the change in impedance, rendering a phase spectrum, amplitude spectrum, and a Nyquist plot.

When the board is plugged in, the microcontroller code writes the registers in the waveform generator and waits for a signal from Matlab. The Matlab code opens a serial port and writes a character. This write indicates that Matlab is ready to receive the data. Once the microcontroller receives this character, it pulses a pin on the waveform generator and produces a sine wave of 100 Hz. The input and the output of the electrodes are fed to two analog pins on the microcontroller. These signals are alternatively digitized and the values are stored in the ADC buffer. A frequency dependent delay is programmed between consecutive sampling points on each signal; this ensures that 20 points are samples for every period of the sine wave. A total of 100 sampled points from each signal and 5 characters representing time information is sent to Matlab. Matlab waits till the buffer contains 210 characters; once the buffer is full, Matlab reads

the value and saves it in a matrix. The matlab code runs this in a loop for 100 times to collect data for 100 frequencies (100 Hz to 10 kHz with an increment of 100 Hz).

Once all the data is collected from all frequencies, Matlab analyzes data from one frequency at a time; the code calculates the amplitude of the signal, phase difference between the signals, and change in impedance. For instance, 100 data points corresponding to 100 hz is retrieved from the saved matrix. Using Matlab's inbuilt data interpolation function, 100 points are inserted between each exiting data points; this increases the number of points from 100 to 9901; shown in Figure 25. This increases the resolution of the data, improving the accuracy of amplitude and phase calculations.

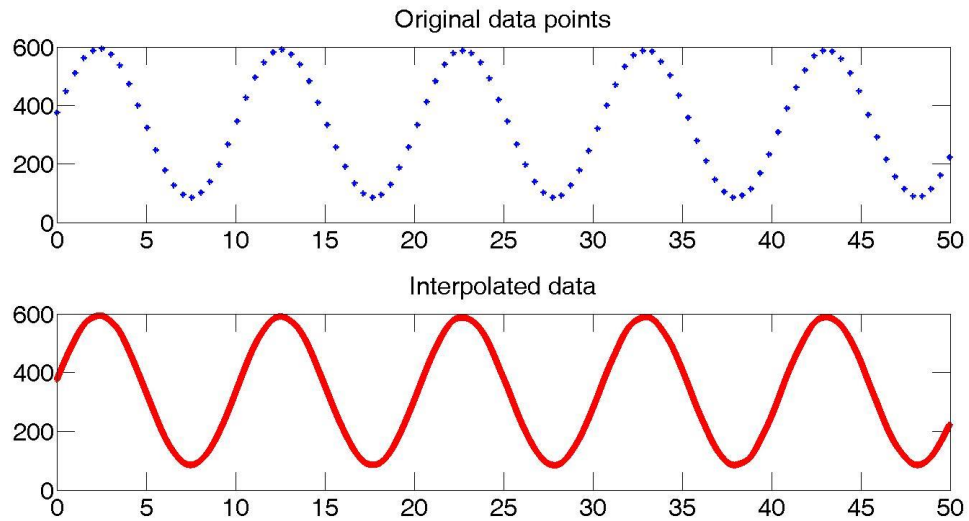


Figure 25 Original data points and interpolated data points

The offset of the signal is determined by calculating the mean of the voltage values. From the mean, the maximum variation from the mean represents the maxima and minima in each period. The average of these values gives the amplitude of the signal. The phase difference between the signals is calculated by measuring the time lag between the maxima points of the

input and output. To calculate this, all data points are given a precise time stamp; the time information sent from the microcontroller is used to determine this value. An array that has the maxima point from each period and the corresponding time stamp information is saved. The maxima points calculated by the code is marked with a black cross in Figure 26.

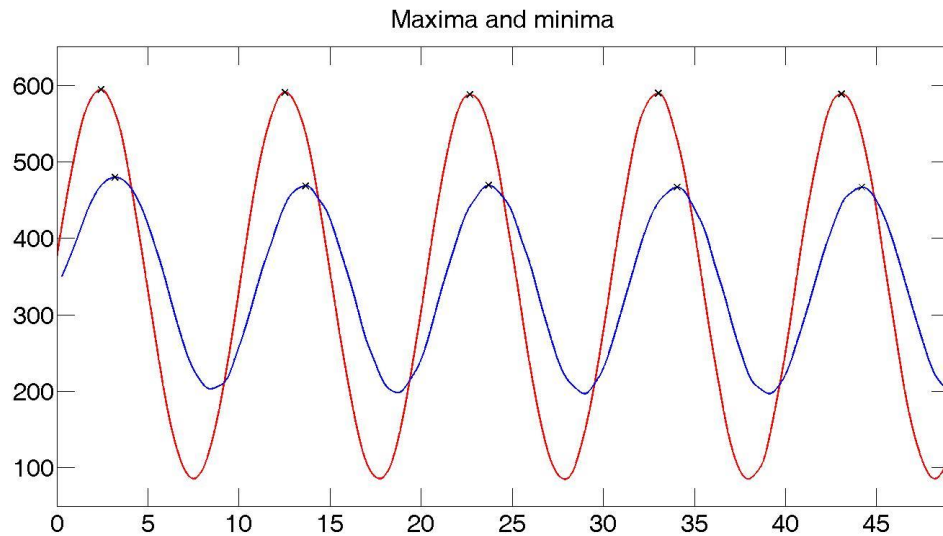


Figure 26 Maxima and minima points on input and output signals

The time difference between the maxima points of the signals in each period is saved. This information is converted to phase difference using the following formula. Phase information from each period is averaged to calculate the phase difference between the signals.

$$Phase = 360 * Frequency * Time\ difference$$

With the phase difference and amplitude information, the impedance of the electrodes are calculated using the following equations,

$$Real = Z * \cos \theta$$

$$\text{Imaginary} = Z * \sin \theta$$

Where,

$$Z = \frac{V_{out} * 1000}{V_{in} - V_{out}}$$

θ = phase difference

4.5 Results

Before integrating the system, the subsystems of the device were tested using traditional lab equipment to validate their functionality. The performance of the integrated system was tested by measuring change in impedance with different samples. Amplitude spectrum, phase spectrum, and Nyquist plots from data collected using the proposed device is presented in this section.

4.5.1 Saline solution

For preliminary testing, bare gold electrodes were exposed to saline solution of different concentrations. The change in amplitude and phase spectrum with different concentrations of sodium chloride was recorded. Three concentrations of 0.1M, 0.5M, and 1M NaCl solutions were prepared and 20 μ L of the salt solution was dispensed on the electrodes during the tests.

Theoretically, solutions with high salt content conduct better than salt solutions with low salt concentrations. Hence, the resistance measured from 0.1M NaCl must be highest and the resistance of 1M should be the lowest. The Nyquist plot should also show a similar trend; the plot should shift and increase as the concentration increases. The data shown in Figure 27 agrees with the hypothesis.

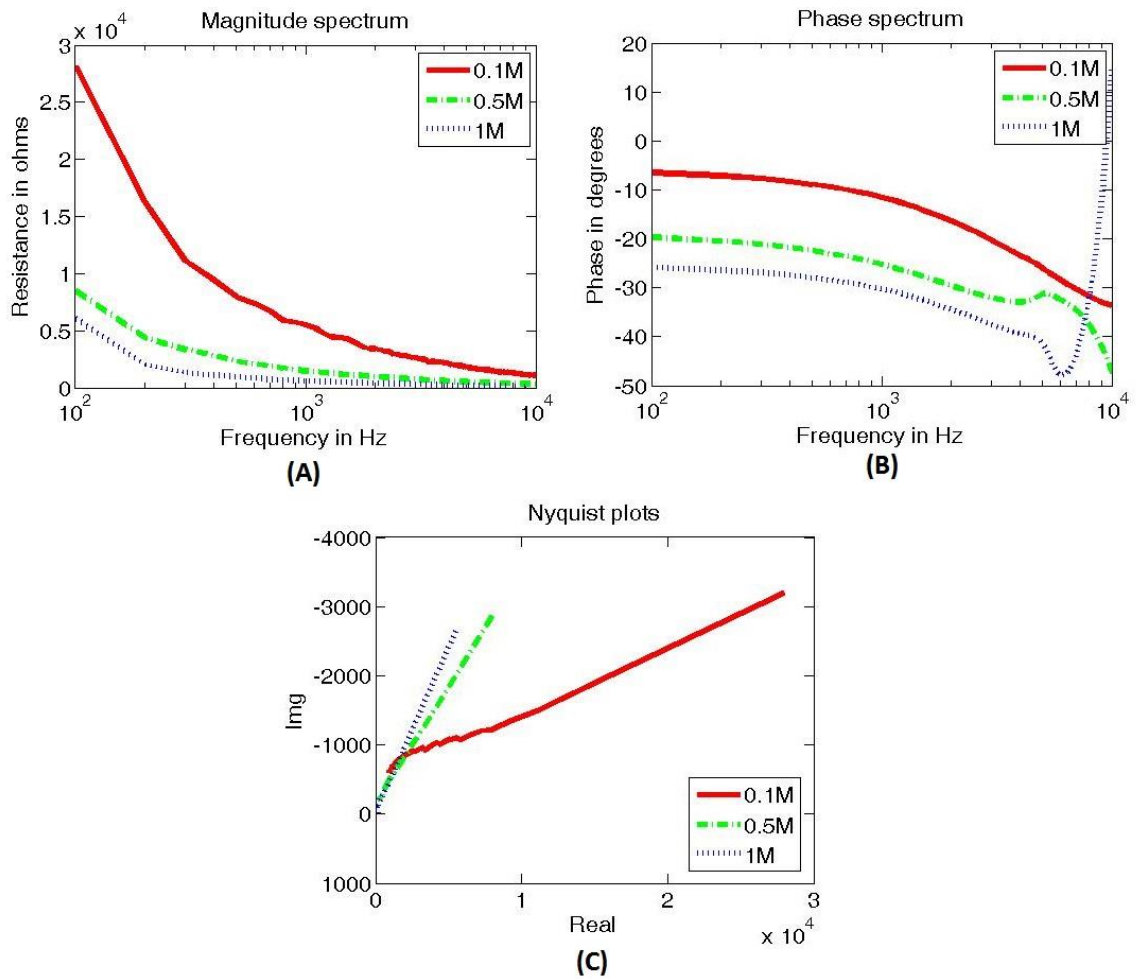


Figure 27 EIS results from NaCl with different concentrations (A) Amplitude spectrum (B) Phase spectrum (C) Nyquist plots

To ensure that the system is working with an acceptable accuracy, the data collected from the device was compared to data from an oscilloscope. The input and output waveforms were sent to the microcontroller and simultaneously measured using an oscilloscope. The scope measured the amplitude and phase difference of the signals. The values that Matlab calculated with the data sent from the microcontroller was compared to the values from the oscilloscope; data is shown in Figure 28.

To conduct this experiment, EIS was conducted by dispensing 20 μ L of 0.1M NaCl on bare gold electrodes. The output amplitude and phase difference were measured at discrete frequencies using the scope. The device was then used to run EIS for the complete frequency range of 100 Hz to 10 kHz.

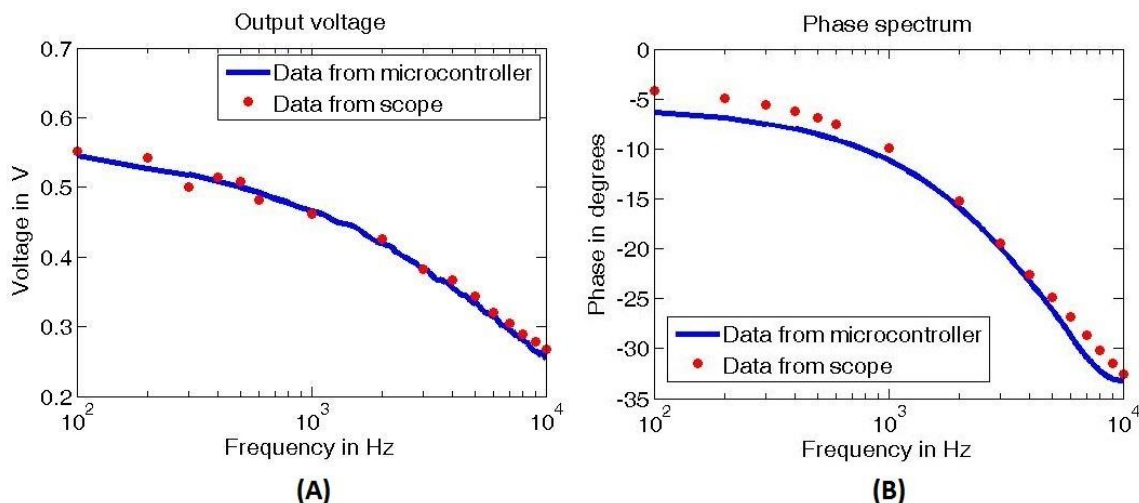


Figure 28 Plots comparing the values from an oscilloscope and the proposed device (A) Output voltage (B) Phase difference

From the data, it can be observed that the amplitude and phase difference calculated with data from the device has a high correlation with the data from the scope. The error in phase difference could be due to the effects of using wires to measure the sine waves on the board. The phase value displayed on the scope also displayed a variation of about 3°-5°. This effect increases as the frequency of sine wave increases.

4.5.2 Protein detection

Protein detection was performed on functionalized gold electrodes. The electrodes were treated with the thiol group to form SAM on the gold surface. 20 μ L of DI water was dispensed on

top of bare gold electrodes and electrodes treated with thiol group to record the change in contact angle [72]. Figure 29 shows a decrease in the contact angle confirming the formation of SAM on the gold.

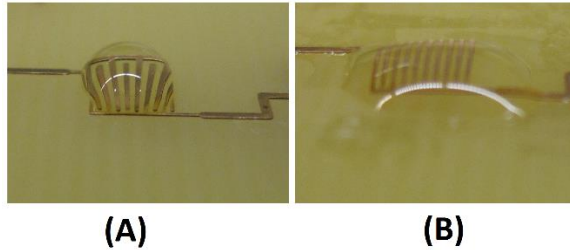


Figure 29 Contact angle on gold surface (A) Bare gold electrodes (B) Gold electrodes after the formation of SAM

To conduct EIS, 20 μL of PBS was dispensed on gold electrodes treated with SAM. The data from these electrodes were collected and saved in Matlab. The same set of electrodes were exposed to GFP, and measured with PBS. Change in values before and after protein binding are shown in Figure 30. SAM layer on gold should increase the conductivity and reduce the measured resistance [73]. As expected, the resistance of SAM is much lower compared to salt solution on bare electrodes. When the protein binds to the SAM, it inhibits conduction leading to an increase in resistance as shown in Figure 30 (A).

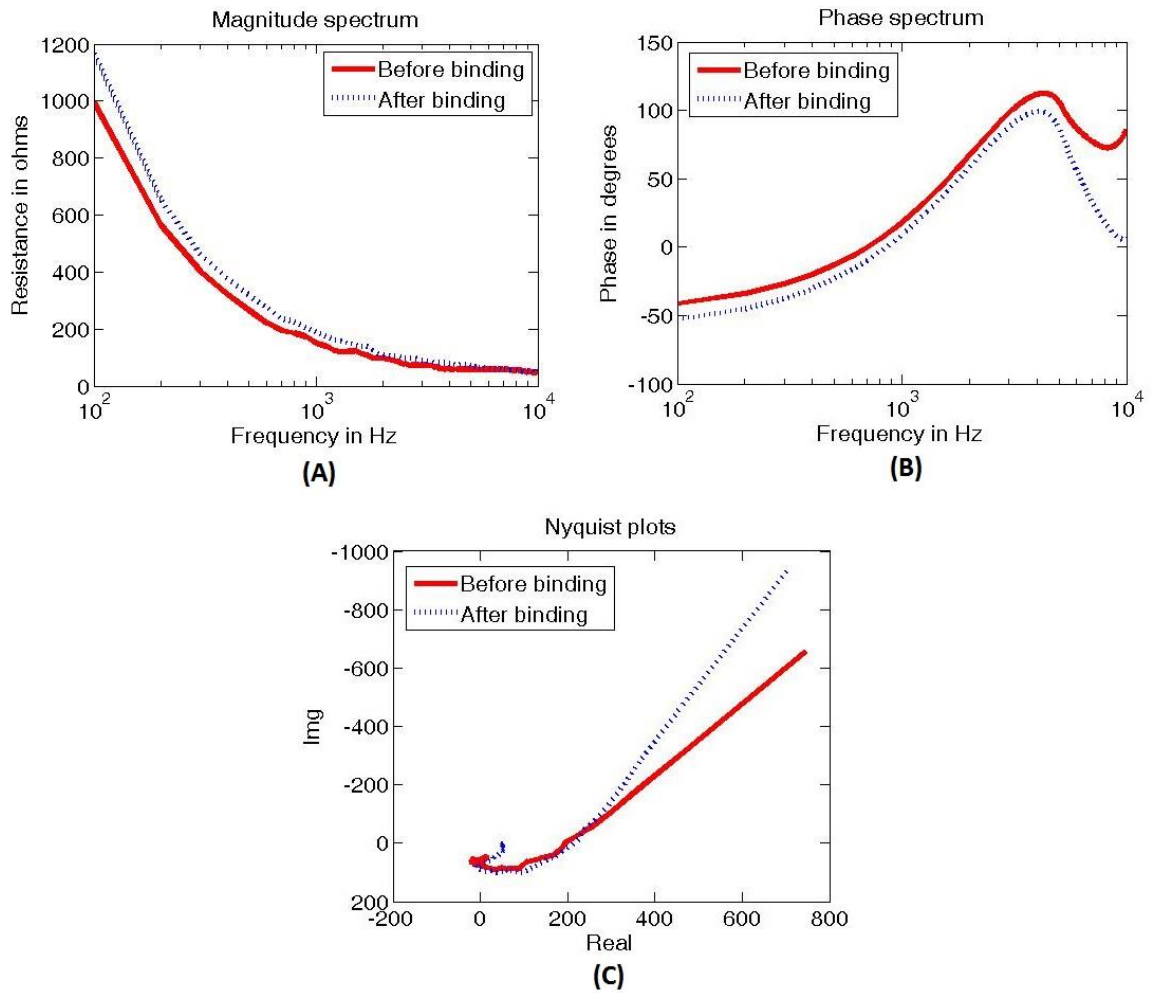


Figure 30 Protein detection using proposed device (A) Amplitude spectrum (B) Phase spectrum (C) Nyquist plot

To calculate the error margin, multiple data sets from a single electrode was collected before and after treating them with the protein. The data was analyzed in Matlab and a graph with error bars was generated; shown in Figure 31. The impedance difference at low frequencies (higher x axis values) is distinct before and after binding. As the frequency increases, the error bars overlap; this could be associated to the phase variations noticed at high frequencies.

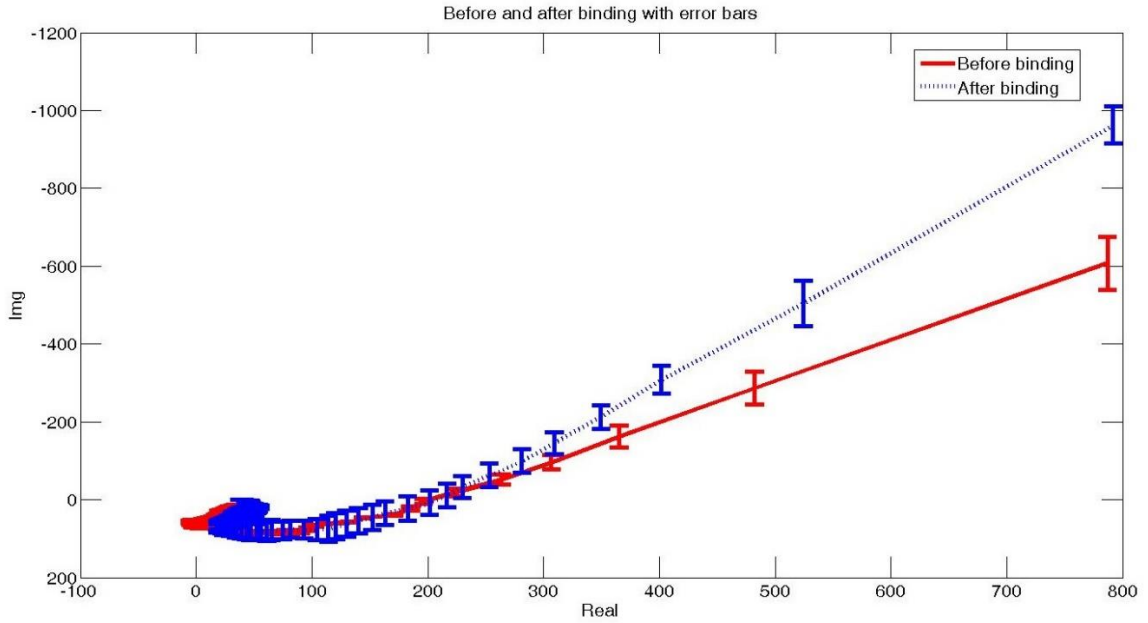


Figure 31 Error margin before and after protein detection

4.5.3 Protein detection with commercial electrodes

When the size of the target molecule decreases, the change in impedance also decreases. To verify that the proposed system can adapt to detect smaller biological samples, the system was integrated with commercial electrodes. Interdigitated gold electrodes from Micrux (ED-IDA1-Au) were used to detect the same +36 GFP. The electrodes were treated using the same protocol and the impedance change before and after protein binding is shown in Figure 32.

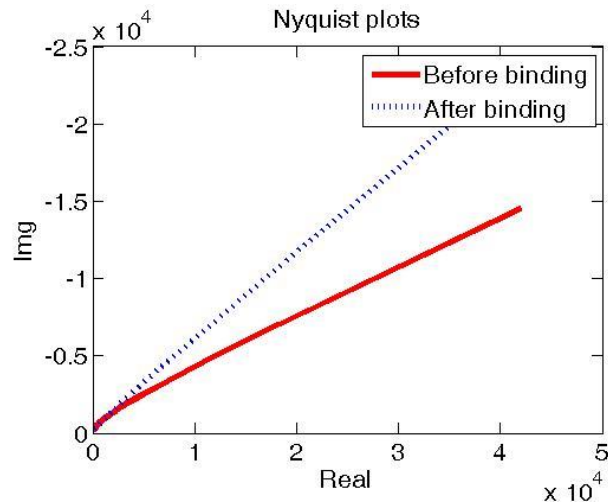


Figure 32 Protein detection using proposed device and commercial electrodes

The impedance difference is one order of magnitude higher than the fabricated electrodes. From this experiment, it is evident that the sensitivity of the system can be improved by using smaller electrodes. Reducing the size of the electrodes confines the electric field closer to the surface of the electrodes which in turn improves sensitivity [72].

4.6 Conclusions

The capability of the device to perform EIS can be extended to screen for HCV by modifying the surface chemistry on the electrodes; this can be achieved by activating the SAM layer and coating the electrodes with antibody that has affinity for HCV antigen and HCV virus. Compared to conventional screening methods, this device would be faster, cheaper, and offer complete screening. The cost of fabricating the electronics PCB and the electrodes PCB was \$67. Since the electrodes are the only part of the device that come in direct contact with the sample, it can be single use and the electronics board can be reused. This would reduce cost per test to about \$20; mass production would further reduce screening costs.

The functionality of this device can also be extended to screen for other diseases by modifying the chemistry. By borrowing the surface chemistry from ELISA kits, the electrodes can be coated with antibody that has affinity for any target molecules. This exponentially increases the number of diseases that can be screened simultaneously using the proposed device.

CHAPTER 5

CONCLUSION

Point of care devices and hand held health monitoring devices have already started to be a part of lives. We hope that the techniques and systems presented in this thesis help push the envelope of this field.

The microfluidic fabrication techniques presented here have been validated by integrating the devices with optical and electrochemical sensors. The proposed fabrication techniques can be applied to numerous miniaturized sensors and devices for sample handling and manipulation. The fabrication techniques can also be employed to develop microfluidic devices with advanced functionalities such as mixing, focusing, and filtering.

The optical and electrochemical systems presented in this thesis not only overcome drawbacks of existing clinical screening methods, but also has the potential to improve current state of technology. The ability of the optical system to detect flowing sample could improve throughput by 100x. This would shed light on sample analysis and open doors to what had been impossible or laborious in the past. Chemical FETs can be developed on CMOS sensors and integrated with microfluidic devices to develop a completely new range of sensors. These devices can offer optical and chemical information about the sample under investigation.

The electrochemical sensor not only offers rapid and low cost screening but has the potential to revolutionize mass screening. By integrating technologies such as near field communication (NFC) device, screening can not only be fast, but completely automated and

secure. In this new model, individuals being screened would fill out their personal details and medical form on their phone or tablets. At screening booths, the data from their phones would be transferred to the passive NFC tag on the PCB. Along with the data from the test, the information from the electronic forms also gets transferred to the computer. An application on the computer would automatically save the individual's personal records and the result of the test. When healthcare providers screen individuals for HCV, they must report a positive case to the state; the software could do this automatically. The software could also send counselling information and information about the disease over emails or messages to the individuals.

The functionality and potential of such point of care devices are numerous. The new generation of miniaturized devices would also help in transforming the traditional model of going to hospitals for medical care and screening. Early detection of diseases and continuous health monitoring would pave way for a healthier tomorrow.

REFERENCES

- [1] Darlene Berger, "A brief history of medical diagnosis and the birth of the clinical laboratory", 1999 <http://www.academia.dk/Blog/wp-content/uploads/KlinLab-Hist/LabHistory1.pdf>
- [2] Common screening and diagnostic tests, U.S Department of Health and Human Services
- [3] Matthew J Thompson, Ann Van den Bruel, "Diagnostic test toolkit", Oxford, 2012
- [4] Deaths and mortality, CDC, <http://www.cdc.gov/nchs/fastats/deaths.htm>
- [5] Power of prevention, CDC, <http://www.cdc.gov/chronicdisease/pdf/2009-power-of-prevention.pdf>
- [6] Jonathan Donner, Patricia Mechael, "mHealth in Practice Mobile technology for health promoting in the developing world", 2014
- [7] Towards the Development of an mHealth Strategy, A Literature Review, WHO, 2007
- [8] Alexandros Pantelopoulos, Nikolas G. Bourbakis, "A survey on wearable sensor-based systems for health monitoring and prognosis", IEEE transaction on systems, 40 (1), 2010
- [9] The global market for medical devices, 5th Ed. A Kalorama Information Market Intelligence Report
- [10] J. Cooper McDonald, David C.Duffy, Janelle R. Anderson, Daniel T. Chiu, Hongkai Wu, Oliver J. A. Schueller, George M. Whitesides, "Fabrication of microfluidic systems in poly(dimethylsiloxane)" Electrophoresis, 21, 27-40, 2000
- [11] Elmabruk A. Mansur, Ye Mingxing, Wang Yundong, Dai Youyuan, "A State-of-the-Art Review of Mixing in Microfluidic Mixers" Chinese Journal of Chemical Engineering, 16(4), 503-516, 2008
- [12] Sung Hwan Cho, Jessica M.Godin, Chun-Hao Chen, Wen Qiao, Hosuk Lee, Yu-Hwa Lo, "Review Article: Recent advancements in optofluidic flow cytometer" Biomicrofluidics 4, 043001, 2010
- [13] Tabeling, Patrick, "Introduction to Microfluidics" Oxford, GBR: Oxford University Press, UK, 2006. ProQuest ebrary. Web. 11 September 2014, ch1, pp.2-21
- [14] Yeshaiahu Fainman, Demetri Psaltis, Changhuei Yang, "Optofluidics: Fundamentals, Devices, and Applications" The McGraw-Hill Companies, ch.2, pp.7-13, 2010
- [15] Stephen C. Terry, John H. Jerman, James B. Angell, "A Gas Chromatographic Air Analyzer Fabricated on a Silicon Wafer", IEEE, 26(12), 1880-1886, 1979

- [16]A. Manz, "Miniaturized chemical analysis systems based on electroosmotic flow", IEEE MEMS, Nagoya, Japan, 26-30, 1997
- [17]M. Despont, H. Lorentz, N. Fahrni, J. Brugger, P. Renaud, P. Vettiger, "High-aspect ratio, ultrathick, negative-tone near-UV photoresist for MEMS applications" IEEE MEMS, 162-167, 1996
- [18]Srinath Satyanarayana, Rohit N. Karnik, Arunava Majumdar, "Stamp-and-Stick Room Temperature Bonding Technique for Microdevices" Journal of Microelectromechanical systems, 14(2), 2005
- [19]Jennifer Blain Christen, Andreas G. Andreou, "Design, Fabrication, and Testing of a Hybrid CMOS/PDMS Microsystem for Cell Culture and Incubation" IEEE Biomedical Circuits and Systems, 1(1), 2007
- [20]Ling-Sheng Jang, Chun-Ching Wu, "Fabrication of microfluidic devices for packaging CMOS MEMS impedance sensors" Microfluidics and Nanofluidics, 7, 869-875, 2009
- [21]Lee Hartley, Karan V. I. S. Kaler, Orly Yadit-Pecht, "Hybrid Integration of an Active Pixel Sensor and Microfluidics for Cytometry on a Chip" IEEE Circuits and Systems, 54(1), 2007
- [22]Ebrahim Ghafar-Zadeh, Mohamad Sawan, "A hybrid Microfluidic/CMOS Capacitive Sensor Dedicated to Lab-on-Chip Applications" IEEE Biomedical circuits and systems, 1(4), 2007
- [23]Sangjun Moon, Hasan Onur Keles, Aydogan Ozcan, Ali Khademhosseini, Edward Haeggstrom, Daniel Kuritzkes, Utkan Demirci, "Integrating microfluidics and lensless imaging for point-of-care testing" Biosensors and Bioelectronics, 24, 3208-3214, 2009
- [24]Sungkyu Seo, Ting-Wei Su, Derek K. Tseng, Anthony Erlinger, Aydogan Ozcan, "Lensfree holographic imaging for on-chip cytometry and diagnostics" Lab on a Chip, 9, 777-787, 2009
- [25] Adhesive research <http://www.adhesivesresearch.com/wp-content/uploads/2013/11/92804-Data-Sheet.pdf>
- [26] Maximilian Focke, Dominique Kosse, Claas Muller, Holger Reinecke, Roland Zengerle, Felix von Stetten, "Lab-on-a-Foil: microfluidics on thin and flexible films" Lab on a Chip, 10, 1365-1386, 2010
- [27] Pulak Nath, Derek Fung, Yuliya A. Kunde, Ahmet Zeytun, Brittany Branch, Greg Goddard, "Rapid prototyping of robust and versatile microfluidic components using adhesive transfer tapes" Lab on a Chip, 10, 2286-2291, 2010
- [28] Andres W. Martinez, Scott T. Philips, George M. Whitesides, "Three-dimensional microfluidic device fabricated in layered paper and tape" PNAS, 105(50), 2008

- [29] Christopher J. Easley, Richard K. P. Benninger, Jesse H. Shaver, W. Steven Head, David W. Piston, "Rapid and inexpensive fabrication of polymeric microfluidic devices via toner transfer masking" *Lab Chip*, 9(8), 1119-1127, 2009
- [30] American Society of Hematology <http://www.hematology.org/Patients/Basics/>
- [31] NIH, National Heart, Lung, and Blood Institute <http://www.nhlbi.nih.gov/health/health-topics/topics/bdt/>
- [32] Jeff W Lichtman, Jose-Angel Conchello, 'Fluorescence microscopy', *Nature methods*, Volume 2, Number 12, DOI:10.1038/NMETH817, 2005
- [33] International AIDS Society: Access to HAART for the developing world The next hurdle: affordable lab monitoring (part1), December 5, 2002
- [34] Robert E. Cunningham, 'Overview of flow cytometry and Fluorescent Probes for Flow Cytometry', *Methods Mol Biol.*, 588:319-26, 2010
- [35] Marion G Macey, Desmond A. McCarthy, 'Flow cytometry: Principles and applications', ISBN-10: 1597454516, 2007
- [36] Jessica Godin, Chun-Hao Chen, Sung Hwan Cho, Wen Qiao, Frank Tsai, Yu-Hwa Lo "Microfluidics and photonics for Bio-System-on-a-Chip: A review of advancements in technology towards a microfluidic flow cytometry chip", *J Biophotonics*, 1(5), 355-376, 2009
- [37] Shiang-Chi Lin, Pei-Wen Yen, Chien-Chung Peng, Yi-Chung Tung, "Single channel layer, single sheath-flow inlet microfluidic flow cytometer with three-dimensional hydrodynamic focusing", *Lab on a Chip*, 12, 3135-3141, 2012
- [38] A. Ozcan, U. Demirci, "Ultra wide-field lens-free monitoring of cells on-chip", *Lab Chip*, 8(1), 98-106, 2007
- [39] Ting-Wei Su, Liang Xue, Aydogan Ozcan, "High-throughput lensfree 3D tracking of human sperms reveals rare statistics of helical trajectories", *PNAS*, 109(40), 16018-16022, 2012
- [40] A. F. Coskun et al., "Lensfree fluorescent on-chip imaging of transgenic *Caenorhabditis elegans* over an ultra-wide field-of-view", *PLoS One* 6, e15955, 2011
- [41] E. P. Dupont et al., "Fluorescent magnetic bead and cell differentiation/counting using a CMOS SPAD matrix", *Sens. Actuators B*, 174, 609-615, 2012
- [42] W. Li et al., "On-chip integrated lensless fluorescence microscopy/spectroscopy module for cell-based sensors", *Proc. SPIE*, 7894, 78940Q, 2011
- [43] A. F. Coskun et al., "Lensfree wide-field fluorescent imaging on a chip using compressive decoding of sparse objects", *Opt. Express*, 18(10), 10510-10523, 2010

- [44] Lee SA, Leitao R, Zheng G, Yang S, Rodriguez A, *et al.*, “Color Capable Sub-Pixel Resolving Optofluidic Microscope and Its Application to Blood Cell Imaging for Malaria Diagnosis”, PLoS ONE, 6(10), 2011
- [45] A.Shanmugam, C.D.Salthouse, ‘Lensless Fluorescence Imaging with Height Calculation’, Journal of Biomedical Optics, 19(1):016002, 2013
- [46] A.Shanmugam, C.D.Salthouse, ‘Microfluidic on CMOS with laser Cut Adhesive Tape’, 225th Electrochemical Society Meeting, Orlando, Florida, 2013
- [47] Hepatitis C: An introductory guide for patients, VA Hepatitis C Resource Centers, <http://www.hepatitis.va.gov/>
- [48] Peter R. McNally, “New CDC Hepatitis C virus (HCV) Screening Policy: One Time HCV-Antibody Testing of the Baby Boomer Generation (born between 1945-1965), Visible Human Journal of endoscopy, 11(2), 2012
- [49] Colin W Shepard, Lyn Finelli, Miriam J Alter, “Global epidemiology of hepatitis C virus infection”, Lancet Infect Dis, 5:558-67, 2005
- [50] A.C. El Khoury, W.K. Klimack, C. Wallace, H. Razavi, “Economic burden of hepatitis C-associated diseases in the United states”, Journal of Viral Hepatitis, 19, 153-160, 2012
- [51] Recommendations for the identification of chronic hepatitis virus infection among persons born during 1945-1965, Centers for disease control and prevention, Recommendations and reports, Vol 61, No 4, 2012, <http://www.cdc.gov/mmwr/preview/mmwrhtml/rr6104a1.htm>
- [52] Sushmita Shivkumar, Rosanna Peeling, Yalda Jafari, Lawrence Joseph, Nikita Pant Pai, “Accuracy of rapid and point-of-care screening tests for hepatitis C”, Annals of Internal Medicine, 157(8), 558-566, 2012
- [53] Marc G. Ghany, Doris B. Strader, David L. Thomas, Leonard B. Seeff, “Diagnosis, Management, and Treatment of Hepatitis C: An Update”, Hepatology, Vol 49, No. 4, 2009
- [54] Recommended testing sequence for identifying current hepatitis C virus (HCV) infection http://www.cdc.gov/hepatitis/hcv/PDFs/hcv_flow.pdf
- [55] HIV and Viral Hepatitis, CDC http://www.cdc.gov/hiv/pdf/library_factsheets_HIV_and_viral_Hepatitis.pdf
- [56] Oraquick, OraQuick <http://www.orasure.com/products-infectious/products-infectious-oraquick-hcv.asp>
- [57] Manit Arya, Neehar Arya, Lyndon Gommersall, Hitendra RH Patel, Iqbal S Sherqill, Magali Williamson, “Basic principle of real-time quantitative PCR”, Expert review of molecular diagnosis, 5.2, pp. 209, 2005

- [58] Dianping Tang, Juan Tang, Biling Su, Jingjing Ren, Guonan Chen, "Simultaneous determination of five-type hepatitis virus antigen in 5 min using an integrated automatic electrochemical immunosensor array", *Biosensors and Bioelectronics* 25, 1658-1662, 2010
- [59] Michael Jacobs, Vinay J. Nagaraj, Tim Metz, Anjan Paneer Selvam, Thi Ngo, Shalini Prasad, "An electrochemical sensor for the detection of antibiotic contaminants in water", *Anal. Methods*, 5, 4325, 2013
- [60] Arun Manickam, Christopher Andrew Johnson, Sam Kavusi, Arjang Hassibi, "Interface Design for CMOS-Integrated Electrochemical Impedance Spectroscopy (EIS) Biosensor", *Sensors*, 12, 14467-14488, 2012
- [61] Kinjal Bhavsar, Aaron Fairchild, Eric Alonas, Daniel K. Bishop, Jeffrey T. La Belle, James Sweeney, T.L. Alford, Lokesh Joshi, "A cytokine immunosensor for Multiple Sclerosis detection based upon label-free electrochemical impedance spectroscopy using electroplated printed circuit board electrodes" *Biosensors and Bioelectronics*, 25, 506-509, 2009
- [62] Pawlotsky, J M, L. Prescott, P. Simmonds, C. Pellet, P. Laurent-Puig, C. Labonne, F. Darthuy, *et.al*, "Serological Determination of Hepatitis C Virus Genotype: Comparison with a Standardized Genotyping Assay" *Journal of Clinical Microbiology* 35 (7), 1734-1729, 1997
- [63] Donna M. Zucker, Jeungok Choi, Emily Gallaher, "Mobile Outreach Strategies for Screening Hepatitis and HIV in High-Risk Populations", *Public Health Nursing*, 29 (1), 27-35, 2011
- [64] D. Zucker, A. Shanmugam, "Point of care HCV screening in jail: A human factor study", *Gastroenterology Nursing*, 40(1), 2017- *Accepted for publication*
- [65] Sunil K. Arya, Ganna Chornokur, Manja Venugopal, Shekhar Bhansali, "Antibody functionalized interdigitated μ -electrode (ID μ E) based impedimetric cortisol biosensor, *Analyst*, 135, 1941-1946, 2010
- [66] Junhong Min, Antje Baeumner, "Characterization and optimization of interdigitated ultramicroelectrode arrays as electrochemical biosensor transducers", *Electroanalysis*, 16 (9), 2004
- [67] R.Zlatev, M.Stoytcheva, B.Valdez, L.Alvarez, J.M.Cobo, "Application of single-use PCB gold disc electrodes for "in-situ" determination of As(III) in natural waters" *ECS Transactions*, 20(1), 3-12, 2009
- [68] Kidong Park, Ho-Jun Suk, Demir Akin, Rashid Bashir, "Dielectrophoresis-based cell manipulation using electrodes on a reusable printed circuit board", *Lab Chip*, 9, 2224-2229, 2009

- [69] Fuchs SM, Raines RT, "Arginine grafting to endow cell permeability", ACS Chem Biol, 2(3), 167-70, 2007
- [70] Michael S. Lawrence, Kevin J Phillips, David R Liu, "Supercharging proteins can impart unusual resilience", JACS, 129(33), 10110-10112, 2007
- [71] Jung Wook Lee, Sang Jun Sim, Sung Min Cho, Jeewon Lee, "Characterization of a self-assembled monolayer of thiol on a gold surface and the fabrication of a biosensor chip based on surface plasmon resonance for detecting anti-GAD antibody", Biosensors and Bioelectronics 20, 1422-1427, 2005
- [72] Zhiwei Zou, Junhai Kai, Michael J. Rust, Jungyoup Han, Chong H. Ahn, "Functionalized nano interdigitated electrodes arrays on polymer with integrated microfluidics for direct bio-affinity sensing using impedimetric measurement", Sensors and Actuators, 136, 518-526, 2007
- [73] Emel Adaligil, Young-Seok Shon, Krzysztof Slowinski, "Effect of headgroup on electrical conductivity of self-assembled monolayers on mercury: n- Alkanethiols versus n- Alkaneselenols", Langmuir letter, 26(3), 1570-1573, 2010